
Politecnico di Torino

Politecnico di Torino

Corso di Laurea Magistrale in Mechanical Engineering

Tesi di Laurea Magistrale

# The dynamics of a wheel loader handling unbound granular material

## FMI-based co-simulation with Simulink and Demify

Relatori:
Tonoli Andrea
Quist Johannes
Lidberg Mathias
Lindmark Elianne
Ekevid Torbjörn
Jareteg Klas

Candidato:
Balla Marsel

A.a. 2020/2021
Ottobre, 2021

Master's thesis 2021

# The dynamics of a wheel loader handling unbound granular material

MARSEL BALLA


Politecnico di Torino

Department of Mechanical and Aerospace Engineering
*Division of Mechanical Engineering*
Politecnico di Torino
Turin, Italy 2021

A machine-particle interaction study via a co-simulation technique
The embodiment of the bucket to rock dynamics in a wheel loader through a coupling method assisted by the use of Functional Mock-up Unit
Marsel BALLA



Supervisor Politecnico di Torino: Prof. Andrea Tonoli, Automotive Engineering
Supervisor FCC: Johannes Quist, Fraunhofer-Chalmers Centre
Examiner: Ass. Prof. Mathias Lidberg, Vehicle Dynamics, Chalmers University of Technology
Supervisor Volvo CE: Torbjörn Ekevid, Volvo CE, Virtual Product Development, Braås
Supervisor Volvo CE: Elianne Lindmark, Volvo CE, Wheel Loader Mechanical and Simulation Engineering, Eskilstuna
Co-Supervisor FCC: Klas Jareteg, Fraunhofer-Chalmers Centre

Master's Thesis 2021
Department of Mechanical and Aerospace Engineering
*Division of Mechanical Engineering*
Politecnico di Torino
IT - 10129 Turin

Turin, Italy 2021

A machine-particle interaction study via a co-simulation technique
The embodiment of the bucket to rock dynamics in a wheel loader through a coupling method assisted by the use of Functional Mock-up Unit

MARSEL BALLA
Department of Mechanical and Aerospace Engineering
Politecnico di Torino

# Abstract

A wheel loader is a heavy equipment used to perform granular material handling operations. The complete machine model is developed in Matlab/Simulink®, meanwhile a discrete element method (DEM) solver, modelling unbound granular materials is developed in Demify®. Virtual development technologies allow for more efficient testing of the machine and its sub-systems. Therefore, the implementation of models between different software is required, though there is a lack of standardized interfaces. At this step, FMUs are the leading component making up for a possible integration between different working environments. The work focuses in creating an interface between the two software so the sharing of information is possible. The granular material was previously modelled with the DEM solver GRAPE, which is based on a spherical shaped particle representation to model soil material. On the other hand, crushed rock aggregates which we are working with, require a well-resolved rock particles' representation of the irregular and angular shape.
A new GPU solver for complex particle shape based on non-convex polyhedral triangulation has been implemented, allowing for high fidelity rock shape representation. In this project, the created FMU files contain the information needed to relief the communication issue between the software and make the co-simulation possible. The DEM solver Demify® provides high fidelity results in terms of material contact force detection, while Multi-Body Dynamics (MBD) Simulink® integrates the equations of motion. The computational performance, involving the computational cost and the physical fidelity, is a pivotal factor used to evaluate and optimise the design of a new level machine-particle interaction. Reliable and computationally effective results are obtained in the interaction between machine and non-convex shaped rock particles. In addition, a realistic and an efficient communication between the two software is reached.

Keywords: FMU, Wheel loader, Demify®, Matlab/Simulink®.

# Acknowledgements

First off, I want to acknowledge the assistance of Johannes Quist, my main supervisor responsible for the scientific research in DEM at FCC. I really appreciate your time and devotion on everything discussed and I consider that, as the pivotal stimulus behind the accomplishment of this thesis work. Also, the support received from my supervisors from Volvo CE, Elianne Lindmark and Torbjörn Ekevid has been exceptional. I want to thank you for your availability and cordiality shown in all the meetings we had. A special gratitude goes also to my examiner from 'Chalmers University of Technology' Mathias Lidberg, for his impeccable and valuable feedback throughout the evolution of this thesis work. Also, I would like to thank my co-supervisor Klas jareteg from FCC, for his much appreciated support in the computer programming fraction of the project. In addition, I want to acknowledge the feedback and cooperation of Andrea Tonoli, my supervisor from 'Politecnico di Torino'.

I also want to thank Volvo CE, FCC and Chalmers University of Technology for providing me the means to work on such an innovative topic. Another thing I want to appraise, is the practical support received from Volvo CE, which has been a main contributor to the achievement of the final prominent results which furtherly back up the use of virtual elaboration technologies.

Finally, I would like to thank all my friends, my cousins and my family for the continuous support during my university career. Their guide and inspiration throughout the years have been crucial towards the success in something, that some years ago seemed highly desirable, but scarcely possible. The ones always recalling me that the key to success is to focus on goals, not obstacles. Thank you!

Marsel BALLA, Turin, October 2021

# Contents

# List of Figures

# List of Tables

# 1
# Introduction

## 1.1 Background

Construction equipment is essential in the infrastructure, mining, and energy sector, where Volvo Construction Equipment is an integral part of the worldwide market. Loaders are heavy equipment used to move or load granular materials such as sand, rock and soil to a different location or into another machine, e.g. an aggregate truck. The modern wheel loader is a four-wheeled articulated loader with hydraulically operated tools such as a bucket in front.

In the Vinnova InfraSweden 2030 project DigiRoad, Fraunhofer-Chalmers Centre (FCC) and Volvo CE have collaborated on modelling unbound granular materials using the discrete element method (DEM) solver Demify®. Virtual development technologies have been an essential method of further developing construction machinery. Virtual representations of the complete machine or delimited sub-systems allow for efficient product development and testing. In order to translate the operation and handling of rock and soil materials to a CAE (Computer-Aided Engineering) framework, Volvo CE has strived towards developing high fidelity models of both the machine and the granular material. Currently, Volvo CE is performing multibody dynamics modelling of the wheel loader mechanics and control using Simulink Multibody. The granular material was previously modelled with the DEM solver GRAPE, collaborating with Fraunhofer ITWM [19]. The solvers were coupled for co-simulation between GRAPE and Simulink using an S-function as described according to Matthias[21] and Burger[20]. The GRAPE solver is based on a spherical representation of the particle material and developed to model soil material specifically. While the approach is well proven for soil materials, crushed rock aggregates require a well-resolved representation of rock particles' irregular and angular shape [25], [24].

InfraSweden 2030 aims to improve the transport infrastructure by funding innovative projects, which aim to obtain ambitious results in the Swedish building and infrastructure industry. The innovation project DigiRoad was initiated in 2018 to develop a novel methodology for modelling rock materials and investigating quality aspects of the key handling processes of unbound aggregates from the quarry to the compacted layers in the road. DigiRoad has been the backbone among other research projects to develop the novel DEM solver Demify®, developed at the computational engineering and design department at Fraunhofer-Chalmers Centre (FCC). Today

Demify® is used for various problems related to powders, rock materials and other particle-based systems [22], [23]. Furthermore, since 2020, a new GPU solver for complex particle shape based on non-convex polyhedral triangulations has been implemented, allowing for high fidelity rock shape representation [1]. This project will develop a coupling technique between Demify® and Simulink for DEM-MBD co-simulation using Functional-Mock-Up Interface (FMI). The idea is motivated by the projected capability of using the complete machine model in Simulink with the high-resolution rock particle model in Demify® and how this would enable design evaluation and optimisation on a new level.

The work also includes developing test procedures to assess the influence of particle shape and sizes of typical crushed materials to be used in the simulations. Also, to better assess the material characteristics, the irregularities and shape of the virtual rock particles need to be captured alongside the typical size distribution.

## 1.2 Load prediction in Construction Equipment

The main notion behind this section is the comprehension of the theoretical methodology tailed with the aim of obtaining the desired results. The use of DEM and the two software, is to relate the granular material characteristics to the wheel loader dynamics. Demify® arises new feasible simulation results, in terms of rock particle quality and physics characteristics representation. On the other hand, Matlab/Simulink® represents the wheel loader mechanical, hydraulic, electrical and electronic components, generating high fidelity simulation results. Hence, finding a link between the two software is of high interest in order to approach better results.

The industry standing behind the use of construction equipment is broad, so there is a research field of high interest. Hence, load quantification is a valuable physical parameter to be studied. To this extent, there have been significant studies aiming to reach various techniques that could be used to understand the dynamics behind a construction machine. Studies show that using computer based simulations with an integration of physical motion laws give promising results [20].

## 1.3 Research outline

There are various research supports where this project could be expanded from. Such different research perspectives are related to particle-based simulation using DEM, automation in construction, multi-body dynamics, road construction, co-simulation and simulation-based design. The outcomes of this project are closely related to the research methods and academic relevance throughout a heedful integration of the initial knowledge to the expected results.

The methodological approach instead, is accompanied by key research questions, which are represented below:

1. The current state-of-the art in the literature as regards DEM-MBD coupling.
2. The critical computation performance aspects in large scale DEM-MBD simulations.
3. Influence of high fidelity rock particle model on the relevant wheel loader operational performance response variables.

In addition, the completion of this project is based upon a list of literature and practical tasks, which are going to be introduced and described in more details in the following chapters. Initially, a thorough scrutiny of Discrete element method, Multi-body dynamics and FMI for co-simulation was performed. This was followed by a supplementary work in modelling and simulation, where multiple DEM simulations in Demify® were performed. Additionally, Simulink Multibody model of a wheel loader and FMI for co-simulation were investigated contemporaneously.

A further quest is the verification and validation phase, where the calibration of the rock material model, the implementation verification tests and supporting case application investigation and validation arise.

## 1.4 Scope and objectives

The goal of this project is to validate a co-simulation solution for Simulink Multibody and Demify®. The accomplishment of the identified goal, is reached by upholding the following objectives.

1. Development of wheel loader model with MBD/DEM co-simulation interface.
2. Verification of the FMI interface.

### 1.4.1 Delimitations

This thesis comprises many research topics, so it is important to confine the research and keep within certain boundaries to limit the extensiveness of the project. The main reason behind it, is to prioritise the core of the thesis to cover the main research topic efficiently. This leads to the following delimitations.

1. No development of the DEM model or related code is planned to be included in the scope. If such actions are needed, the DEM team at FCC will support the project accordingly.
2. The project will not focus on developing experimental data sets of for instance wheel loader bucket load/force data for validation purposes. Such data is expected to be available or generated external to the master thesis project.
3. Existing MBD models of the complete wheel loader will be the core resource for machine modelling. Additional modelling in Simulink will be either simplified configurations or archetypic case configurations for testing and verification.
4. The project does not pinpoint the development of new numerical integration schemes for the co-simulation.

# 2

# Computational granular mechanics

## 2.1 Contact Mechanics

Modelling and designing whole structures or full vehicles is a complex process, since it often leads to difficult and complex equations which require more effort and time to converge to a realistic solution.
Hence, the use of an approach responsible for mapping the dynamics of the system is needed. There are two methods of solving the physics of a system constituted by different particles and bodies. The first one is FEM, acronym for Finite Element Method, and the other one is DEM, acronym for Discrete Element Method. FEM is a numerical solving method which computes at an approximate level the solution of the whole system, by applying the physical laws at relatively small finite elements of the bigger system. Note that, this method could be time inefficient when a huge number of contacts is present.

On the other hand, DEM portrays the bulk in separate rigid bodies, accumulating each single contribution to determine the overall dynamics. Instead, the dynamics between the rigid bodies is simpler as it is solved in an explicit manner assuming binary contacts. This is the most feasible way of retrieving converging results, where a simple trade-off between computation time and reliable results is also considered [11].

Solid Mechanics is a dominant research topic, and contact mechanics is unarguably one of the main subjects behind it. This section illustrates the mechanics between the rigid bodies in contact. It is of high importance to discuss the deformation and the contact area between them, so the transmitted energy into the system could be evaluated. In this work, the energy transmitted between the bucket and the rocks is to be evaluated and investigated. Early studies of DEM were based on Hertzian contact theory, used to find the contact area and the indentation depth between simple geometries, like spheres or cylinders. Alongside it, Hertz-Mindlin-Deresiewicz is another approach used to quantify the dynamics between the rigid bodies, which is the one followed in this work. Hereafter, we set up the integration method of the particle state, where we use a second-order explicit Verlet velocity method.

In addition, Newton's second law is another fundamental concept which is being

used. A completely independent integration of each particle using Newton's second law computes the new state. Equations 2.1 and 2.2 represent the linear and rotational motion of a single rigid body simulated. Thornton[14] gives a thorough insight of the particle kinematics, which is represented below in a compact form.

$$m_i \frac{d^2\vec{x}_i}{dt^2} = \sum_j \vec{F}_{ij}^{contact} + \vec{F}_i^{gravity} \tag{2.1}$$

where we could see the mass $m_i$, the translational acceleration $\frac{d^2\vec{x}}{dt^2}$, the gravitational force $\vec{F}_i^{gravity}$ and the contact force due to the neighbouring rigid body j, $\vec{F}_{ij}^{contact}$.

$$I_i \frac{d\vec{\omega}_i}{dt} = \sum_j \vec{M}_{ij} \tag{2.2}$$

where we introduce the mass moment of Inertia $I_i$ of each rigid body i, followed by the variation in time of the rotational velocity $\vec{\omega}_i$ and the reacting moment $\vec{M}_{ij}$, rigid body j has on rigid body i.

In order to solve the system of equations a second order Verlet Velocity scheme is applied, which is a method used to integrate the Newton's equations of motion. Referring to this technique, Grønbech – Jensen[26] introduces Equations 2.3 and 2.4 which are used to calculate the position $\vec{x}$ and velocity $\vec{v}$ of a rigid body at a frequency equal to the value of the DEM time-step $\Delta t_{DEM}$. Both of the equations are represented for the sole reason of illustrating the integration of the equation of motion 2.1.

$$\vec{x}_i(t + \Delta t_{DEM}) \approx \vec{x}_i(t) + \vec{v}_i(t)\Delta t_{DEM} + \frac{1}{2}\vec{a}_i(t)\Delta t_{DEM}^2 \tag{2.3}$$

where $\vec{x}_i(t)$ is the position of particle i at time t, $\vec{x}_i(t + \Delta t_{DEM})$ is the new position of particle i at time $t + \Delta t_{DEM}$ , $\Delta t_{DEM}$ is the DEM time-step and $\vec{a}_i(t)$ is the acceleration of particle i.
Whereas the acceleration of particle i at time $t + \Delta t_{DEM}$ could be derived from the interaction using the particle position $x_i(t + \Delta t_{DEM})$, hence dependent on the contact force and position of particle i.

$$\vec{v}_i(t + \Delta t_{DEM}) \approx \vec{v}_i(t) + \frac{\vec{a}_i(t) + \vec{a}_i(t + \Delta t_{DEM})}{2}\Delta t_{DEM} \tag{2.4}$$

where $\vec{v}_i(t)$ is the velocity of particle i at time t, $\vec{v}_i(t + \Delta t_{DEM})$ is the new velocity of particle i at time $t + \Delta t_{DEM}$ and $\vec{a}_i(t + \Delta t_{DEM})$ is the acceleration of particle i at time $t + \Delta t_{DEM}$.

On the other hand, MBD involves the integration of both translational (2.1) and rotational equation of motion (2.2). In addition, it is fundamental to state the importance of the DEM time-step $\Delta t_{DEM}$ and MBD step size $\Delta t_{MBD}$ when considering the stability of the simulation. On one hand, the time step size should not be too high, since it might lead to jagged results, not being able to detect all of the contacts occurring between the rigid bodies. Also, choosing a very small time step

is not favorable in terms of computational performance. The latter would lead to very accurate results, but inefficient overall computational performance. Its selection procedure is to be addressed to Section 3.2.1, where possible $\Delta t_{DEM}$ are introduced.

## 2.2 Material Geometry

Geometry plays an important role when running a simulation, since it is directly related to the computational cost and the results reliability. The more complex it is, the more reliable the results would be, but accompanied with a substantial computational cost increase. This statement, stimulates a compromised solution between the computational cost and the results fidelity. Bilock[1] introduces the typical rigid body geometry representations in DEM. That is where the core of this work is based on. The most common geometry representations are spheres, multi-spheres and polyhedrons. The latter could be depicted as a convex or non-convex shaped polyhedron. Below the possible geometries are briefly introduced.

Spheres - A relatively simple geometry, generating high computational advantages, compared to the other two cases. Its simple geometry stands as a valid reason for being used, so the interaction is depicted easily enough. Hertzian contact is a method used to detect the contact and the force distribution.

Multispheres - An incorporation of sub-spheres. Bilock[1] introduces an overall conception behind the use of this model. The spheres are bundled together so they act as a full rigid body. The contact instead is detected at an individual scale, regarding each sub-sphere individually. The latter gives rise to accumulation of contacts which lead to higher contact forces, defining an overlapping volume generating non-converging results as could be seen in Bilock's[1] work.

Convex and non-convex polyhedrons - The computational effort needed to calculate the contacts present becomes a real problem when it comes to simulating millions of rigid bodies. Also, the detection approach could lead to distortion of the force magnitudes. Anyhow, this is the leading geometry to very reliable results. Hence, a non-convex polyhedron geometry is what we also use.

After, this brief introduction to the possible rigid body geometries, we have a clearer idea of what could give more efficient results. Figure 2.4 shows a synopsis of the aforementioned geometrical representations and directs us to the most appropriate geometry selection, by maintaining a good trade-off between computational effort and physical reliability.

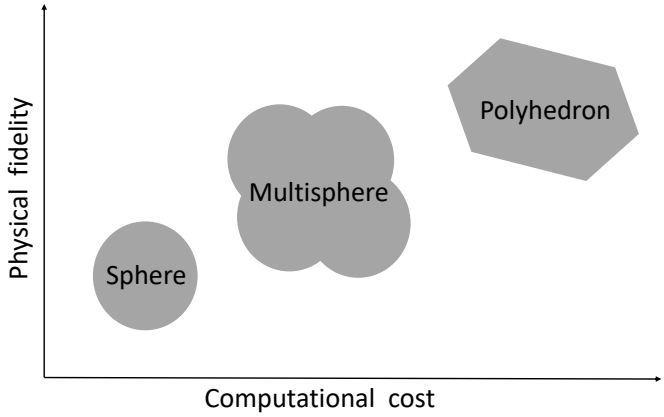


**Figure 2.1:** A graphical illustration of the relation between the computational cost and physical fidelity of the different rock geometries, introduced in Section 2.2.

The figure shows a linear increase of the computational cost with the physical fidelity. This gives rise to one of the main research questions behind this work, concerning, the most suitable geometry we could use. The geometry selected is the non-convex polyhedron, which has proven to be a fairly good example as could also be seen from Figure 2.2.

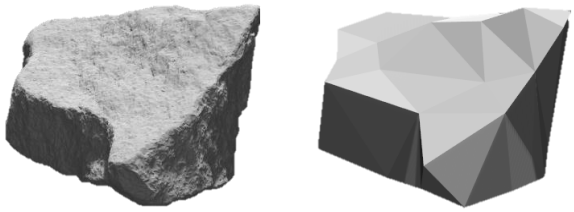

**Figure 2.2:** Representation of a real rock in the left, alongside its virtual representation via Demify based on non-convex polyhedral triangulation in the right.

## 2.3 Contact detection

The geometric problem arising behind contact detection is a topic of interest. The main scope is to use the most appropriate methods so complex physical systems motion is represented in an effective and simplified way. Contact could be easily identified when using spherical geometries, but the contact detection becomes quite challenging when the complexity increases. The main goal is to reach a proper contact detection method, so we refer to studies already being accomplished. Figure

2.3 indicates the steps followed in order to detect the contact and retrieve the data for each rigid body i, until we reach the end of the simulation. Another factor worth mentioning is the time-step $\Delta t_{DEM}$ which is further discussed in the next sections.

Bilock[1] reports a detailed work verifying the physics followed to detect the contact, at various levels of shape irregularities, discussed also in section 2.2. As regards the physics, Govender[4] explains in a thorough extent the technique to the contact detection. A technique composed of two phases, the broad and the narrow one. The former deals with an estimation on potential contacts between two polyhedrons, whereas the latter does a more detailed job in filtering for contacts.

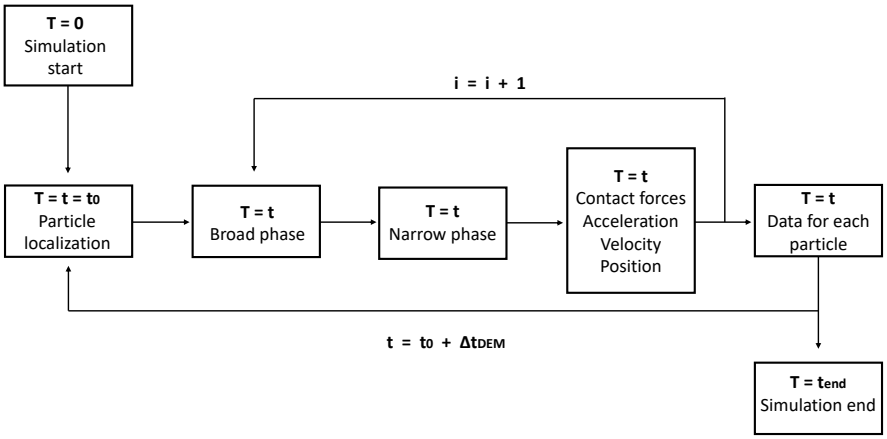


**Figure 2.3:** The steps performed by the algorithm to map the contact mechanics. Note that particles are denoted by i and incremented by 1 until the simulation ends, accompanied by an incremental time step $\Delta t_{DEM}$.

Wilke[7], Bilock[1] and Govender[4] explain how the contact is retrieved following the broad and narrow phase approach.
The broad phase simplifies the complexity by considering 2 rigid bodies i and j as possibly being in contact. The narrow phase verifies if the two rigid bodies are in contact, which could be edge-to-edge, face-to-face or vertex-to-face.The latter is determined on whether an overlapping volume is present. Figure 2.4 shows a 2-D drawing of 2 simple polyhedrons i and j, and their overlapping area.

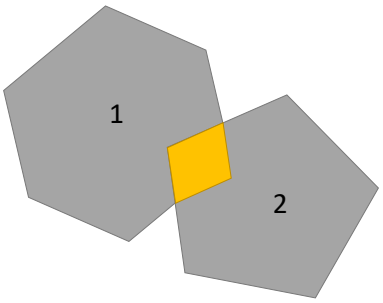


**Figure 2.4:** A 2D representation of the overlapping area of two polyhedrons in contact with each other.

Contact forces between the particles and the particles and the rigid objects are resolved on the basis of the Hertz-Mindlin-Deresiewicz (HMD) force. Now let us introduce the Equations used to get the normal and tangential force. Equation 2.5 represents the formula used to get the elastic normal force.

$$F_{n,e} = \frac{4}{3} E^* R^{1/2} \delta^{3/2} \tag{2.5}$$

where $F_{n,e}$ is the elastic force in the normal direction, $E^*$ is the effective modulus, which is computed as shown in Equation 2.6, R is the effective radius and $\delta$ is the overlapping distance.

$$\frac{1}{E^*} = \frac{1-\nu_1^2}{E_1} + \frac{1-\nu_2^2}{E_2} \tag{2.6}$$

where $\nu$ is the Poisson's ratio. Instead when it comes to computing the effective radius in case of polyhedrons relation expressed in Equation 2.7 is used.

$$V \approx \pi \delta^2 R \tag{2.7}$$

where V is the overlap volume.

Another normal force is the dissipative one, which is computed as can be seen from the Equation 2.8 shown below.

$$F_n = \frac{4}{3\sqrt{\pi}} E^* \sqrt{V\delta} + 2\gamma \sqrt{m^* k_n} v_n \tag{2.8}$$

where $m^*$ is the effective mass, $\gamma$ is the proportionality constant between the friction force and the velocity, $v_n$ is the normal velocity and $k_n$ is the normal spring constant, which both are computed using the relations below.

$$k_n = 2E^* \sqrt{R\delta}$$
$$m^* = \frac{m_1 m_2}{m_1 + m_2}$$

On the other hand, when it comes to the tangential force computation Equation 2.9 comes to help by first introducing the elastic tangential force.

$$\begin{aligned} F_{t,e}^n &= F_{t,e}^{n-1} + k_t^n \Delta\delta_t \qquad \text{if } \Delta F_n \geq 0 \\ F_{t,e}^n &= F_{t,e}^{n-1} \left( \frac{k_t^n}{k_t^{n-1}} \right) + k_t^n \Delta\delta_t \qquad \text{otherwise} \end{aligned} \tag{2.9}$$

where $k_t$ is the tangential spring constant and $G^*$ is the effective shear modulus. Instead, both are solved by using the expressions below.

$$k_t = 8G^*\sqrt{R\delta},$$

$$\frac{1}{G^*} = \frac{1-\nu_1^2}{G_1} + \frac{1-v_2^2}{G_2} = \frac{2(1-v_1)}{E_1} + \frac{2(1-v_2)}{E_2}$$

To sum up the tangential force term, the total tangential force is introduced, and it could be evaluated using Equation 2.10.

$$\begin{aligned} F_t &= F_{t,e}^n + 2\gamma\sqrt{m^*k_t}v_t \\ \text{if } F_t < \mu F_n & \\ F_t &= \mu F_n \\ \text{otherwise} & \end{aligned} \tag{2.10}$$

where $\mu$ is the friction coefficient, $F_{t,e}$ is the elastic tangential force and $F_t$ is the total tangential force.

## 2.4 Particle size and Distribution

Particle Size Distribution often referred as PSD, is an important parameter dealing with the allocation of the material over a specified size range. Packing density, being the fraction of space made up by the material of interest, is affected by the PSD. In the evolution of different simulations, it is one of the main parameters to vary in order to see the resulting differences.

# 3

# Wheel loader handling granular material

## 3.1 Multi-body machine dynamics

A wheel loader is a construction machine which requires accurate physical representation. It is composed of a driving and hydraulic system, which make the physics complex. Although, developing a proper full model machine could be challenging, it is of high industrial interest to improve the mathematical and physical models. This is where Multi-Body Dynamics (MBD) comes into play. Hence, the study of MBD is of high interest due to its capability of relating ideas to computer simulations, and so retrieving cost efficient and fast feedback.
In order to have a visual interpretation of the wheel loader, Figure 3.1 comes to help with a view in the x – z plane.

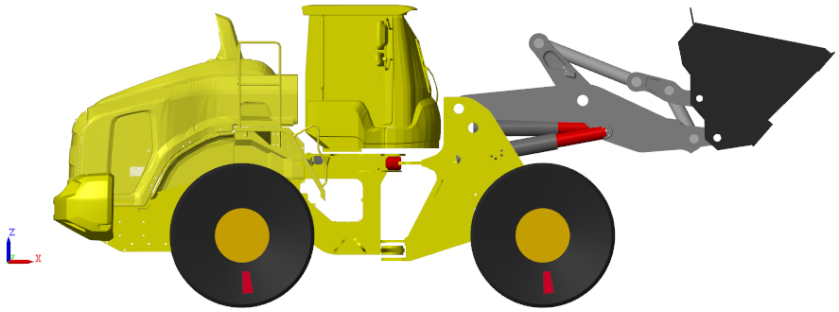

**Figure 3.1:** A representation of the full wheel loader model in Simulink. This is the wheel loader which is to be used for the co-simulations performed in Section 5.

The focus of this work is framed at representing the dynamics of the bucket in a multi-body system environment is the main domain of interest. Kim[8] introduces the components making up the wheel loader and gives validated results in terms of energy flow analysis, which match the real dynamic characteristics of the wheel loader.
At this step, it is essential to show the interaction between the rocks and the bucket. This could be done by performing different loading operations of the bucket with respect to the material being handled. That being said, we could perform a vertical or horizontal loading operation of the bucket into a pile of rocks, and hereafter

conduct an investigation on the retrieved physical response of the system, which is furtherly discussed in Chapter 5. Instead, Figure 3.2 illustrates a 2D drawing of the rocks and the bucket. In addition, forces present due to the motion of the bucket into the pile of rocks are indicated.

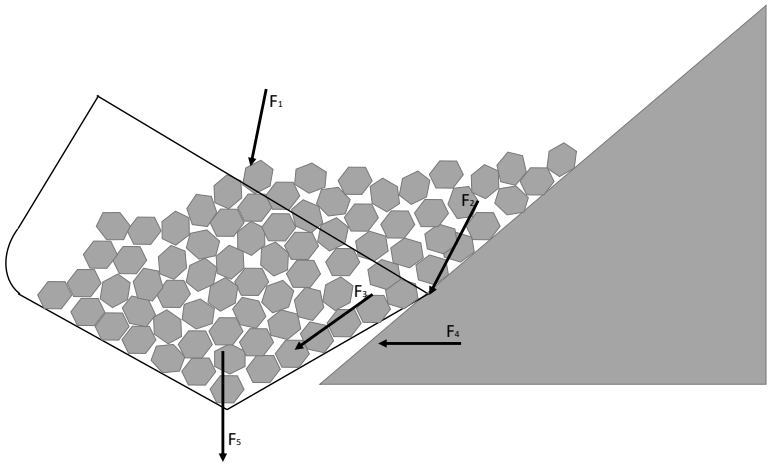


**Figure 3.2:** A 2D representation of a simplified bucket model interacting with simple 2D rock particle geometries.

The arrows present in the figure represent the different forces in place. The force of the rocks moving inside the bucket is denoted by $F_1$, followed by the force applied at the bucket tip as $F_2$. On the other hand, $F_3$ represents the force due to friction, meanwhile $F_4$ is related to the force the bucket experiences in the bottom face. Instead, $F_5$ represents the gravitational force, which sums up the force investigation in this 2-D system.

Chapter 2.1 introduces the law of motion, concerning the rigid body dynamics. In addition, Henriksson[16] gives a detailed investigation of the physics standing behind it.
Equations 3.1 and 3.2 represent the force equilibrium in direction x and y.

$$F_x = F_{1x} + F_{2x} + F_{3x} + F_4 \tag{3.1}$$

$$F_y = F_{1y} + F_{2y} + F_{3y} + F_5 \tag{3.2}$$

This is where the DEM solver starts the force detection and evaluation between the rigid bodies in contact.

## 3.2 Discrete element modelling of granular material

### 3.2.1 Time-step

One of the main parameters during the simulation phase is the time step. It is the principal factor when trying to map the dynamics and create the connection between

the rigid bodies. This comes due to the quick changes of the contact forces, in other words due to disturbances present in the system. So, we could intuitively say that the smaller the time step the better and the smoother the results are. Theoretically speaking this approach works fine, but practice shows that the smaller the time step, the more computationally difficult it becomes to reach a converging result. Thornton[14] comes into play with a quite good approximation on a term *known as* the critical time step. The latter is based on the minimum particle size and we pick a value lower than what obtained from Equation 3.3.

$$\Delta t^{c}_{DEM} = \frac{\pi R_{min}}{v_R} = \frac{\pi R_{min}}{\lambda}\sqrt{\frac{\rho}{G}} \tag{3.3}$$

where $R_{min}$ is the minimum rock radius, $\rho$ is the rock density, G is the rock shear modulus, $v_R$ is the Rayleigh wave speed and $\pi$ is the constant.

In addition the last term, $\lambda$ can be obtained by solving Equation 3.4 and then approximating it to Equation 3.5, where $\nu$ is the Poisson's ratio.

$$(2-\lambda^2)^4 = 16(1-\lambda^2)\left[1-\lambda^2\left(\frac{1-2\nu}{2(1-\nu)}\right)\right] \tag{3.4}$$

$$\lambda = 0.8766 + 0.1631\nu \tag{3.5}$$

Thornton[14] uses this technique to have a threshold when it comes to choosing a good time step. Referring to this method reliable results could be obtained, but as mentioned beforehand the time step directly affects the computational cost, so even in this case an overall trade-off between computational effort and time step size is performed. Table 3.1 relates the time step to the stability of the system, hence the coordination number. This allows for a selection of the critical time step value $\Delta t^{c}_{DEM}$.

| Coordination number | $\Delta t_{DEM}$ |
|---|---|
| High | $\backsim 20\% \cdot \Delta t^{c}_{DEM}$ |
| Low | $\backsim 40\% \cdot \Delta t^{c}_{DEM}$ |

**Table 3.1:** An insight on choosing an appropriate value of $\Delta t_{DEM}$ in accordance with the Coordination number.

On the other hand, Table 3.2 shows possible $\Delta t^{c}_{DEM}$ and $\Delta t_{DEM}$ values of a trial case, where $R_{min} = 0.060$m, $\rho = 1000\frac{kg}{m^3}$, G = 40MPa, $\nu = 0.25$ and $\lambda = 0.91$.

| Critical time-step values | $\Delta t_{DEM}$ |
|---|---|
| $\Delta t^{c}_{DEM}$ | $10^{-3}$ [s] |
| $20\% \cdot \Delta t^{c}_{DEM}$ | $2 \cdot 10^{-4}$[s] |
| $40\% \cdot \Delta t^{c}_{DEM}$ | $4 \cdot 10^{-4}$[s] |

**Table 3.2:** Possible DEM time-step $\Delta t_{DEM}$ values with reference to the critical DEM time-step $\Delta t^{c}_{DEM}$ values.

## 3.3 The machine-particle interaction

### 3.3.1 FMI co-simulation

In many engineering fields there is a need of implementing models between different software, but at the same time there is a lack of standardized interfaces. In other words, models done in one tool are needed in another tool, but there is no bridge to make the process happen. This is where inefficiencies come into play, and we relate to performed studies to this problem. Studies show that fragile and missing interfaces are part of most problems in getting processes inefficient and not fast enough to work. The goal is to simulate a complete system, between different modelling and simulation environments. This implies that different components have to interact with each other, leading to a common solution which backs up the use of a standard interface. This is where the so called Functional Mock-up Unit interface comes into play. The idea behind it is to have fully integrated systems, where is possible to share information. We could also denote it as a steering member, which reliefs the communication issue between the different software.

In the previous sections it is introduced the theory behind the DEM and the MBD. Now, it is time to address the coupling between the two. DEM provides us with high fidelity results in terms of material contact force detection, while MBD integrates the equations of motion where we could simulate the dynamical behavior of the equipment.

### 3.3.2 Co-simulation setup

This section represents the outline of the main work behind the thesis. Figure 3.3 illustrates the three main elements so a valid co-simulation is reached. It starts with a case simulation run in IPS Demify. This simulation generates results which could be read in a python environment. Note that, we could also skip the simulation in Demify, by typing in the code in Python right away. This python file is then adjusted and integrated with a python slave file, latter used to create the fmu file. A Windows PowerShell script is than used to obtain the fmu file. Once the fmu is created, it could be integrated in a simulation performed in Matlab/Simulink. The

communication between the DEM and MBD continues, since the DEM introduces the forces to the system and on the other hand MBD updates the position and velocity of the equipment. This implies that the final result is similar to a loop where each of the components updates the other, so a feasible behavior of the machine and of the particles is obtained.

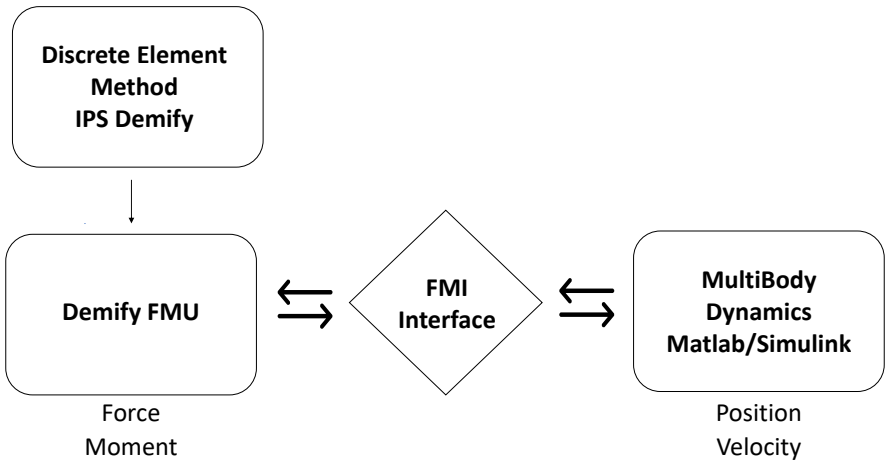


**Figure 3.3:** Visual interpretation of how the communication between the two software occurs. The FMU stands as a bridge in the middle of the two environments, "translating" and updating the information needed for the co-simulation. It supplies Simulink with force/moment data from IPS and supplies the latter with motion/rotation updates from Simulink.

Table 3.3 labels the procedure followed in a 6-step method.

| | |
|---|---|
| 1 | IPS Demify simulation |
| 2 | Python code script |
| 3 | Slave python script |
| 4 | FMU generation from Windows PowerShell |
| 5 | Import fmu file to simulink |
| 6 | Run the simulation |

**Table 3.3:** The steps followed to reach the final results.

Once the technique to be followed is introduced the main goal is focusing the attention at verifying the physics of the obtained results. An iterative procedure is the main tackling mechanism to better understand the impact of the different parameters present in the simulation.
The main purpose of this section is to further validate the stability of the co-simulation, thus different set-up cases are performed. Lommen[18] shows a qualitative work, when it comes to coupling and co-simulating two software in a DEM-MBD interface. It assures the importance of the time step when it comes to performing different simulations. This is to be additionally verified in the simulations performed in Chapter 4 and 5.

# 4

# Model verification

## 4.1 System dynamics of falling rocks

This is the first verification simulation, where rocks are falling into a box in the IPS Demify environment. The reason why a box is chosen is because it could be considered as a simple model of the bucket itself. Figure 4.1 represents the geometry of the box used in the simulations which follow in the next sections. The goal is to get a feedback on the physical parameters, such are force applied in the vertical direction and particle population kinetic and potential energy. After evaluating these parameters, the obtained results convergence is discussed. The reasoning behind this procedure is to reach reliable and time efficient results. Keeping this in mind, Section 4.1.1 and 4.1.2 give a further insight into a proper value selection for $\Delta t_{DEM}$ and $\Delta t_{MBD}$.

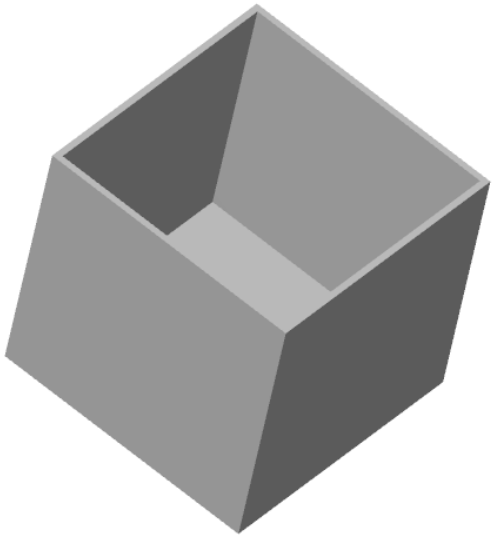

**Figure 4.1:** A 3-D representation of the box used for the first verification simulations, where it is considered as a simplified model of the bucket.

### 4.1.1 DEM time-step analysis

The technical procedure is the same as the one described in Section 3.3.2, the only changes made regard the environment set-up.
In this example a *.fmu* file is initially created and then imported in Simulink. This simulation is performed a few times varying only the DEM time-step, and checking the convergence of the results.

The premise is that of choosing the most suitable $\Delta t_{DEM}$ in terms of results solidity and computational cost. This is why we perform different simulations at different $\Delta t_{DEM}$ size. The verification tests initiate at a range of $10^{-4}$s, behind which stands the theory introduced in Section 3.2.1.

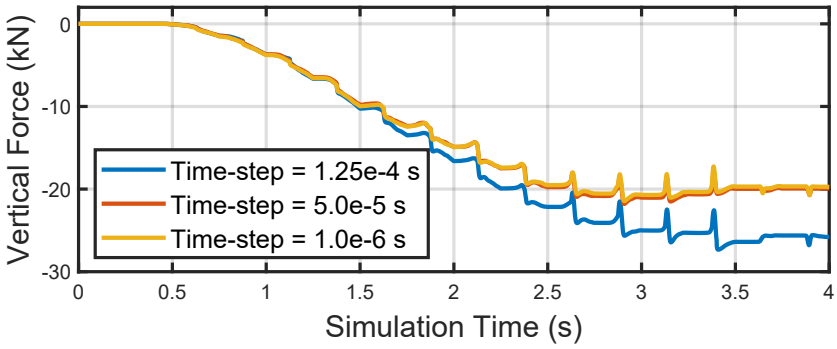


**Figure 4.2:** Force applied on the box in the vertical direction at different DEM time steps $\Delta t_{DEM}$.

Figure 4.2 represents the forces exerted in the system in the vertical direction at different DEM time steps. A divergence could be seen when a relatively big time step is chosen, which could be the blue curve representing a time step value of $\Delta t_{DEM} = 1.25 \cdot 10^{-4}$s. Instead, when a range of $10^{-5}$s is reached the convergence of the results seems more feasible. In this case, we introduce around 2000 kg of material into the box. Also, nothe that the spikes are an effect of the particle-particle dynamics, so when they crash with each other creating lifting for short instants, and in addition to this to instabilities issues.

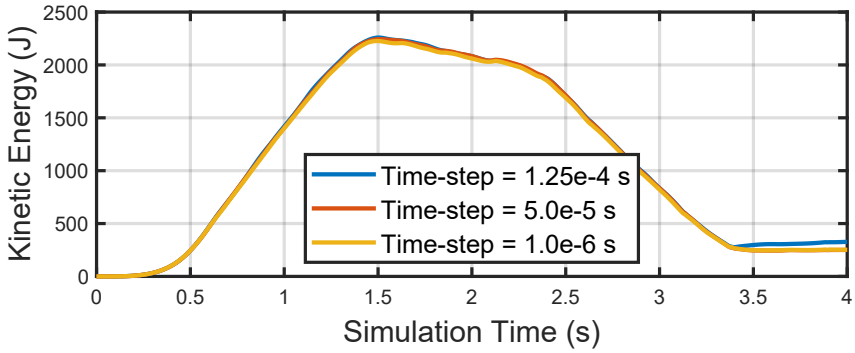


**Figure 4.3:** Particle Kinetic Energy present in the system at different DEM time steps $\Delta t_{DEM}$.

The curve represented in Figures 4.3 and 4.4 illustrate the energy levels at the evolution of a simulation of a duration of 4 seconds. The particles fall within 0 to 2 s time-lapse, and as we can see from the figures they reach high values of energy when the particles hit the surface of the box and then each other during the remaining time. After all the rocks have fallen, there is still energy present in the system, which tends to find a convergent trend as we can see in the respective figures.

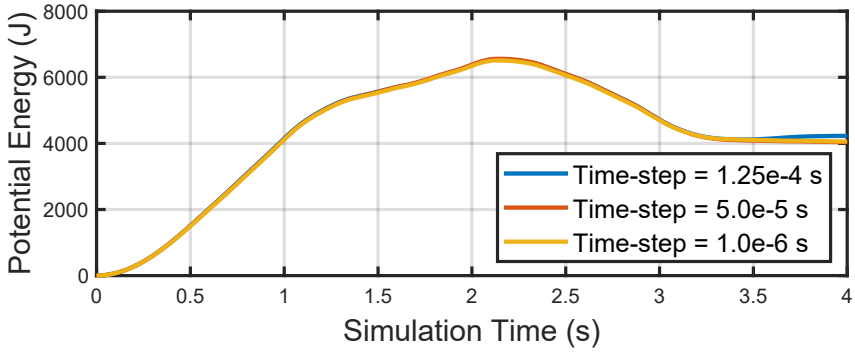


**Figure 4.4:** Particle Potential Energy present in the system at different DEM time steps $\Delta t_{DEM}$.

Figures 4.2, 4.3 and 4.4 illustrate the force exerted in the box in z-direction, Kinetic and Potential energy. At this part of the project we focus on evaluating the convergence and reliability of the results. Keeping in mind that at a lower $\Delta t_{DEM}$ the convergence of theory and reality is more alike. Hence, a lower floor reference $\Delta t_{DEM} = 1.0e-6$ is possible. The verification of the obtained results starts with checking whether the physical parameters values fulfill the law of motion and conservation of energy. This is followed by evaluating a suitable value for $\Delta t_{DEM}$.
To this extent, the error distribution comes to help. The reference point is set as the one with the lowest $\Delta t_{DEM}$. Figure 4.5 is of high importance since it answers to one

of the first questions, the retrieval of reliable results with relatively low computation time, which eases the system effort and requirement.

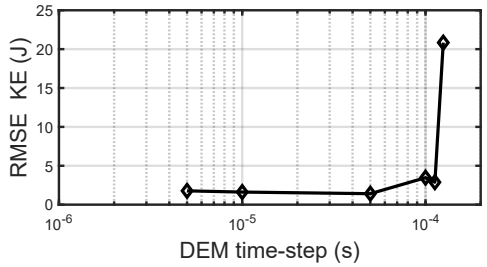


(a) Kinetic Energy error.

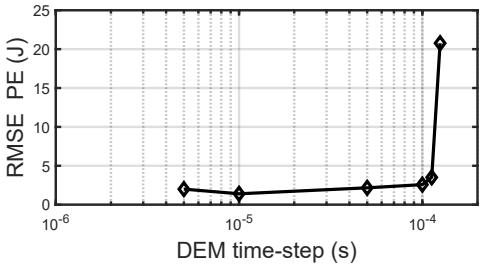


(b) Potential Energy error.

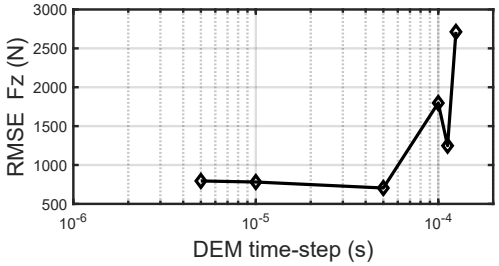


(c) Vertical Force error.

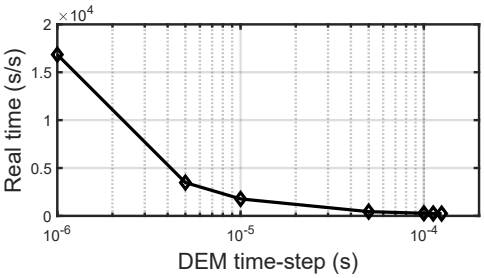


(d) Simulation time dependence.

**Figure 4.5:** Root mean square errors of Force in the vertical direction, Kinetic and Potential Energy and wall clock execution time, used to decide between which of the time-steps $\Delta t_{DEM}$ is the most suitable.

Figures 4.5a, 4.5b and 4.5c label the behaviour of the error, and try to align it with time at a proper $\Delta t_{DEM}$ value. All of the three show a converging trend when the $\Delta t_{DEM}$ is in the range $10^{-5}$ to $10^{-4}$, which also gives the minimum error with respect to the preset reference values from a $\Delta t_{DEM} = 10^{-6}$ (considered as the most reliable one in terms of theory-reality convergence). Anyhow, there is to be highlighted Figure 4.5d which gives a very thorough version of the computational time effort. As expected, the shorter the time-step the higher the wall clock time per simulation tends to be. This being said, now it is time to choose a suitable time-step value which makes up for an acceptable computational fidelity and cost, so a trade-off between the two.
Confronting all the graphs we can come up with a $\Delta t_{DEM} = 5 \cdot 10^{-5}$, which seems to be appropriate at obtaining reliable results and also a good computational effort, so a good wall clock time per simulation time ratio.

### 4.1.2 Co-simulation step size analysis

Simulink step size is the other parameter to be discussed. In a co-simulation, where Simulink is the primary working environment, choosing an abiding value is of high importance. In this case, we perform the simulations directly importing the fmu files in Simulink, where the communication step size $\Delta t_{MBD}$ is tuned, in order to inspect the merging of the curves. As in the $\Delta t_{DEM}$ choice, a high reliability value of $\Delta t_{MBD} = 10^{-3}$s is chosen, hence forces applied on the box alongside the Kinetic and Potential energy are investigated.

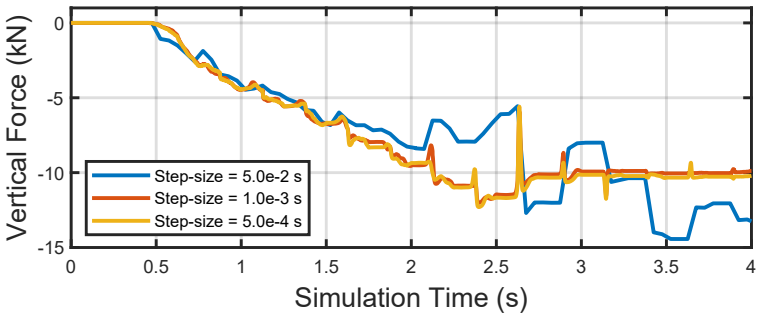


**Figure 4.6:** Force applied on the box in the vertical direction at different MBD step-sizes $\Delta t_{MBD}$.

The communication step size could be related to the rate the system performs the exchange of information, implying that for a higher rate the result quality would be higher, but at the same time would add up a further cost in terms of computational effort and time. As we can see from the Figures 4.6, 4.7 and 4.8, the calibre of the results deteriorates when $\Delta t_{MBD} = 5 \cdot 10^{-2}$s, this leads to another choice. The trend anyhow is positive since the more the value diminishes the more the reliability and uniformity of results increases. Another thing to note down, as mentioned in the time step analysis in Section 4.1.1, are the instabilities of the spikes which are mainly present at high co-simulation step-size values, and this comes due to the quick changes of the contact forces between the rigid bodies. In other words, when the communication time is high, and contact mechanics is complex, then a lot of information is not taken into account, leading to less reliable results, as it could be seen with the blue curve representing a communication step-size of $5 \cdot 10^{-2}$s.

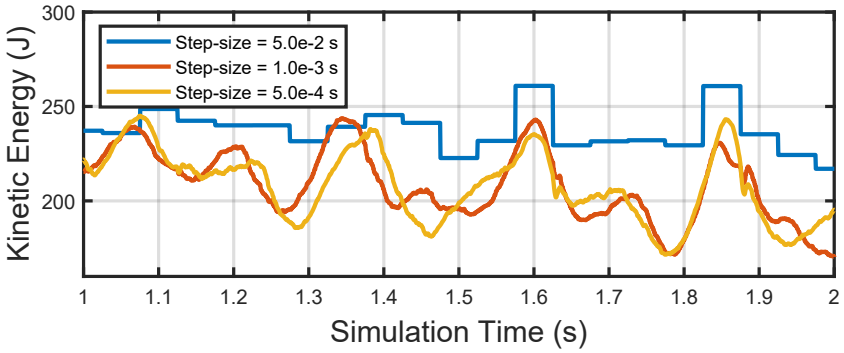


**Figure 4.7:** Particle Kinetic Energy present in the system at different MBD step-sizes $\Delta t_{MBD}$.

Instead, in Figures 4.7 and 4.8 the Kinetic and Potential Energy are represented. Note that in Figure 4.7 a co-simulation time range between 1 and 2 seconds is chosen, even though the simulation time is 4 seconds. This is intentionally done, so the difference between the different communication step sizes is clearly seen. As expected and as formerly explained in the Force graphs, also in the energy representation we have a deteriorating trend when the step-size is at a range of $5 \cdot 10^{-2}$s. Thus, the other communication step-sizes give quite converging results, and smaller errrors, which could also be seen in the error representation in Figure 4.9.

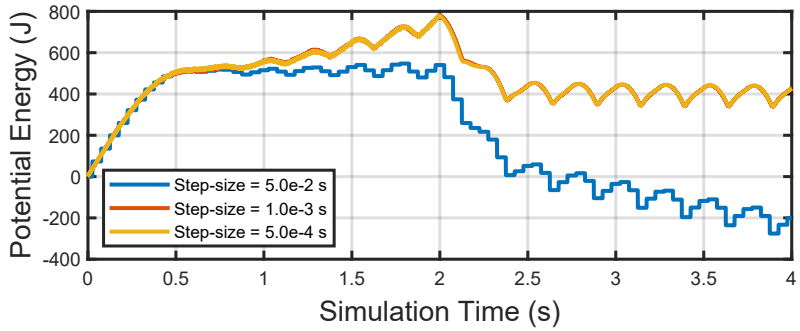


**Figure 4.8:** Particle Potential Energy present in the system at different MBD step-sizes $\Delta t_{MBD}$.

Figure 4.9 instead reproduces a similar approach used in the $\Delta t_{DEM}$ calculation. It is noticeable, that the lower the $\Delta t_{MBD}$ the lower the error is and therefore the better the obtained results we could retrieve are.

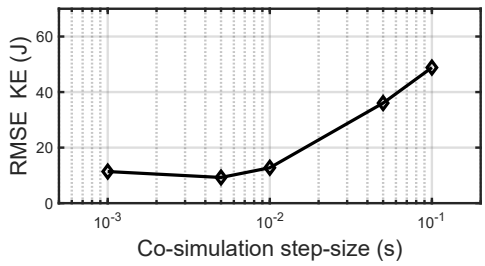


(a) Kinetic Energy error.

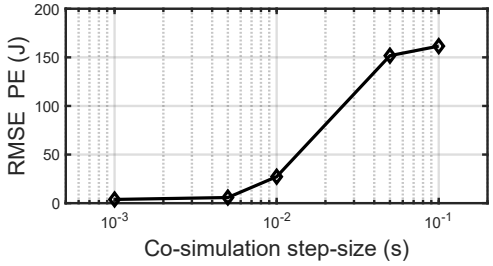


(b) Potential Energy error.

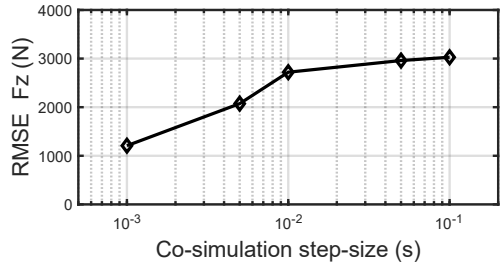


(c) Vertical force error.

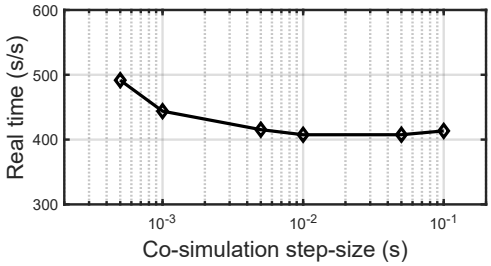


(d) Simulation time dependence.

**Figure 4.9:** Root mean square errors of Force in the vertical direction, Kinetic and Potential Energy and wall clock execution time, used to decide between which of the step-size $\Delta t_{MBD}$ is the most suitable.

Again, a trade-off between the co-simulation step size and the wall clock time needed per performed simulation time is the reasonable approach to be followed, which suggests a value of $\Delta t_{MBD} = 10^{-3}$s.

## 4.2 Falling particles into a box supported by a spring-damper system

It is time to obtain results of a different scale, when it comes to the complexity of the verification case. That is why, we choose to perform the same test of Section 4.1 accompanied by a spring-damper mass system. The simulation consists of rocks falling in a box which is supported by a translational spring and damper. Figure 4.10 shows a simple drawing, where all the components of the simulations which are to be performed are illustrated. In detail, the box supported by a spring(k) and damper(c), the generator from which the rocks are falling from and the respective vertical falling distance (h) could be seen. Note also, the positive direction of the position z(t) and velocity $\dot{z}$(t) of the box over time.

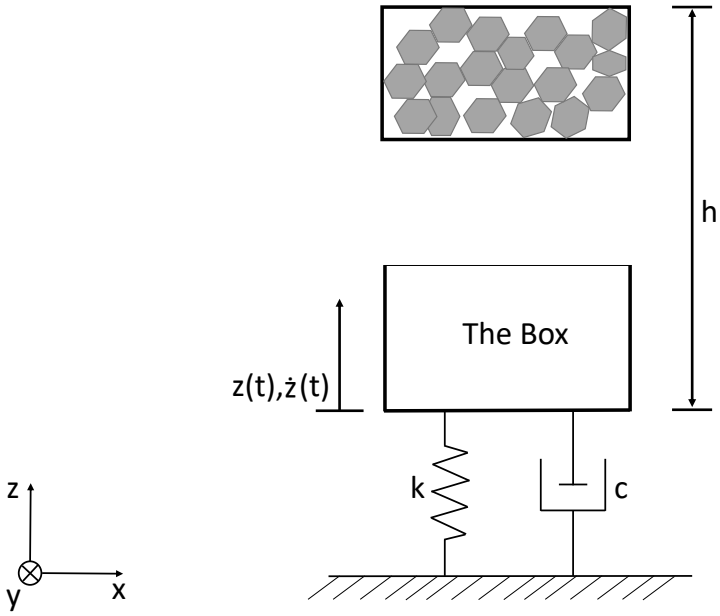


**Figure 4.10:** A drawing which shows the box supported by a spring(k) and damper(c), the generator from which the rocks are falling from and the respective vertical falling distance (h). Note also, the positive direction of the position z(t) and velocity ż(t) of the box over time.

Figure 4.11 shows the particles falling in the box, which results are retrieved after running the simulation in Simulink.

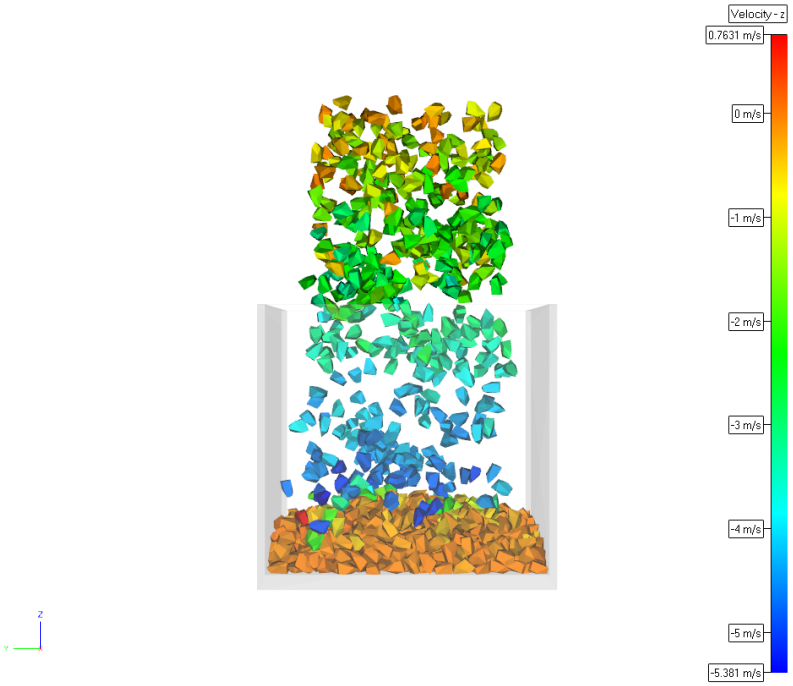


**Figure 4.11:** A visual representation of the rocks falling into the box in the IPS Demify environment. The color of the rocks relates to the velocity magnitude in the vertical direction, which is set as a contour on the side.

The two figures above give just a smooth introduction to what the simulations are being performed on. In this section the focus is to have the convergence of the results fully validated. This is done by varying the simulation parameters so to check the response of the system. The results obtained from Section 4.1.1, confirm the convergence of realistic results at the following time-steps: $\Delta t_{DEM} = 5 \cdot 10^{-5}$s and $\Delta t_{MBD} = 10^{-3}$s.

### 4.2.1 Spring-Damper parameters assessment

In this section, 4 different simulations at different spring stiffness and damping coefficient values are performed.

| Case | 1 | 2 | 3 | 4 | [units] |
|---|---|---|---|---|---|
| Spring stiffness | 32700 | 32700 | 21800 | 21800 | $\frac{N}{m}$ |
| Damper coefficient | 2060 | 1370 | 2060 | 1370 | $\frac{N}{m/s}$ |

**Table 4.1:** Spring and Damping coefficients used for the different demo simulations.

Table 4.1 depicts the values used for the 4 different simulation cases. These values were chosen empirically after stating a specific box positioning in the vertical direction.
The figures hereafter show the obtained results.

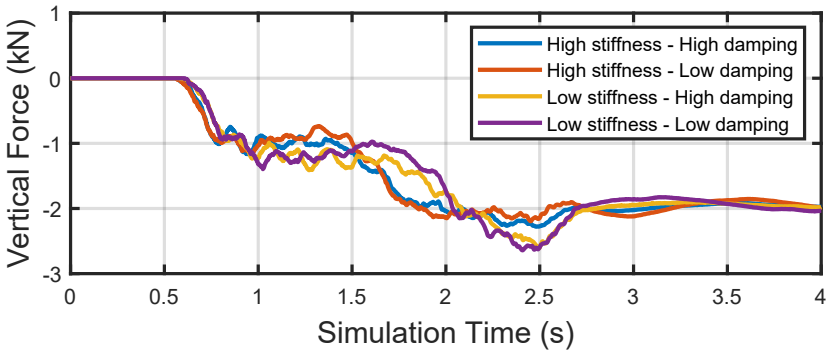


**Figure 4.12:** Force applied to the box in the vertical direction at a time-step $\Delta t_{DEM} = 5 \cdot 10^{-5}$s and a step-size $\Delta t_{MBD} = 10^{-3}$s for different stiffness and damping coefficients.

Figure 4.12 shows that the force is obtained differently in the first 2 seconds when the rocks are falling, and then a converging point is reached when the Kinetic energy in the system is conserved.

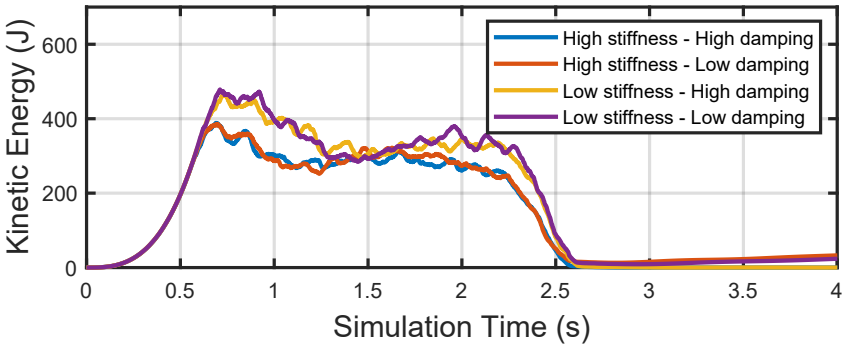


**Figure 4.13:** Total Kinetic Energy of the whole rock particles at a time-step $\Delta t_{DEM} = 5{\cdot}10^{-5}$s and a step-size $\Delta t_{MBD} = 10^{-3}$s for different stiffness and damping coefficients.

Figure 4.13 represents the Kinetic Energy trend during the different simulations performed. Note the dependence that it has to the spring stiffness, where we have similar levels of energy when the spring stiffness is the same, not depending on the damping coefficient. Another thing to note are the repeated spikes in the system which come due to the quick contact forces occurring during the simulation and the dynamics of the rock themselves, making it difficult to have a very smooth curve. Anyhow, the energy levels seem quite feasible, and could be furtherly verified when they reach a converging trend. In addition, during the end of the simulation a divergence tentative of the trend could be seen, and this could happen to the instability of the structure. Another difference could be seen in Figure 4.14 where the variation in the stiffness parameter changes the energy stored by the spring. The dependence in the damping coefficient when it comes to Potential energy is fairly negligible.

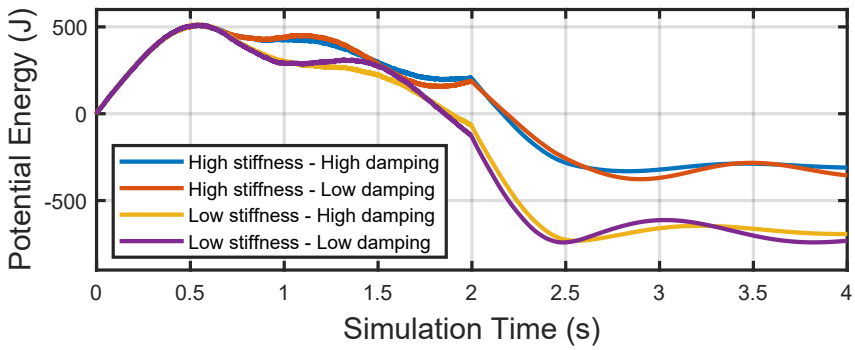


**Figure 4.14:** Total Potential Energy of the whole particles at $\Delta t_{DEM} = 5 \cdot 10^{-5}$s and $\Delta t_{MBD} = 10^{-3}$s for different stiffness and damping coefficients.

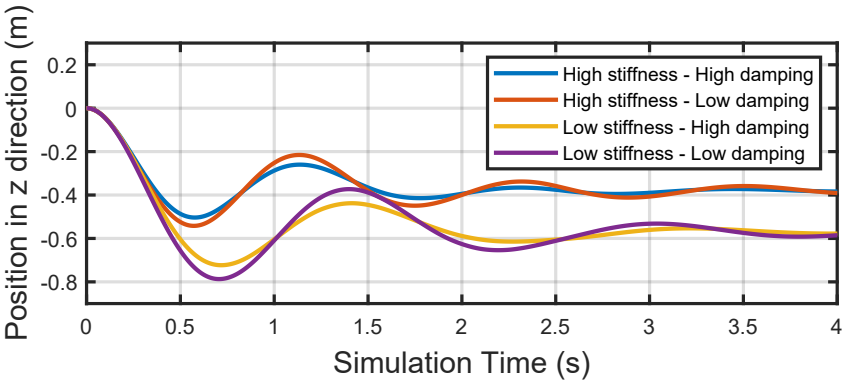


**Figure 4.15:** Position of the box in the vertical direction at a time-step $\Delta t_{DEM} = 5 \cdot 10^{-5}$s and a step-size $\Delta t_{MBD} = 10^{-3}$s for different stiffness and damping coefficients.

In Figure 4.15 instead, the box kinematics to the falling rocks is shown. Here we could detect the convergence of theory into practice, since with a high stiffness value the box moves less in the vertical position. When it comes to damping we could see an amplitude difference only, having to deal with quite similar frequencies. Both Figure 4.15 and 4.16 verify that at a high damping value the energy dissipated is higher, leading to a smother movement of the box, which also implies a lower amplitude.

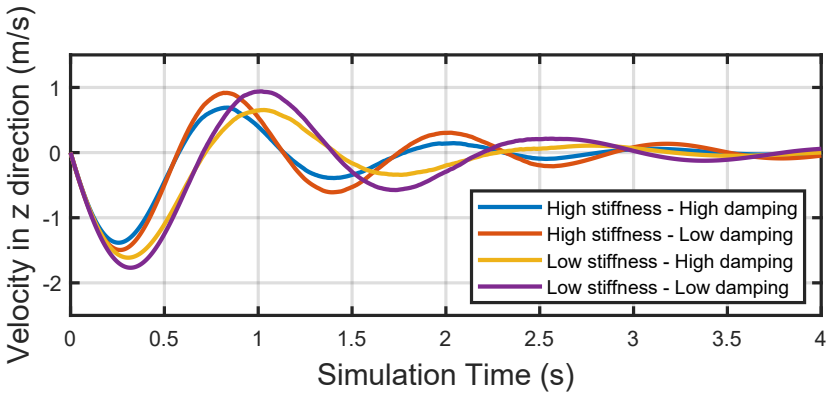


**Figure 4.16:** Velocity of the box in the vertical direction at a time-step $\Delta t_{DEM} = 5 \cdot 10^{-5}$s and a step-size $\Delta t_{MBD} = 10^{-3}$s for different stiffness and damping coefficients.

### 4.2.2 Particle mass variation

It is of interest to check the physics fidelity when different particle masses are introduced into the system. In Section 4.2.1 we refer to a non-varying mass value which is set as $m_{tot} = 200$kg. This time some constant values to the general parameters are assigned. Table 4.2 depicts the constant values which were used in the following simulations.

| | |
|---|---|
| $\Delta t_{DEM}$ | $5 \cdot 10^{-5}$ s |
| $\Delta t_{MBD}$ | $10^{-3}$ s |
| Box density | 1000 kg/m$^3$ |
| Particle mean radius | 0.075 m |
| Young's modulus | 100 MPa |
| Translational spring stiffness | 25000 $\frac{N}{m}$ |
| Damping coefficient | 2000 $\frac{N}{m/s}$ |

**Table 4.2:** Constant parameters for the simulations, which results can be seen in Figures 4.18, 4.19, 4.20, 4.21 and 4.22.

The 3 simulations run at a different mass entering the system, where each mass is respectively $m_1 = 300$kg, $m_2 = 500$kg and $m_3 = 700$kg.
Introducing various masses also brings up to the variation of other parameters. In order to have a balanced and non-oscillating system we need to check also the damping ratio. Various damping scenarios are possible, which include undamped, under-damped, critically damped and over-damped system. This condition is determined by the oscillations exerted onto the system and the damping ratio, denoted by $\zeta$. The latter being the ratio between the damping coefficient and the critical damping coefficient. We tend to have an under-damped scenario in the simulations, where the parts hit back and forth the spring-damper system after each loop, until the available energy in the system dies. In the initial simulations in Section 4.2.1, a damping ratio $\zeta = 0.16$ is used, which is kept constant also in the next simulations.

$$\zeta_c = 2\sqrt{Km} \tag{4.1}$$

where $\zeta_c$ is the critical damping coefficient, K is the spring constant kept at a constant value of 32700 $\frac{N}{m}$ and m is the mass introduced in the system.
Then we use the predefined damping ratio to obtain an appropriate damping coefficient value for each of the introduced masses, as shown in Table 4.3.

| m [kg] | $\zeta_c$ [$\frac{Ns}{m}$] | $\zeta$ [$\frac{Ns}{m}$] |
|---|---|---|
| 1367.5 | 13374 | 2140 |
| 1567.5 | 14318 | 2292 |
| 1767.5 | 15204 | 2433 |

**Table 4.3:** The damping coefficient magnitude for each of the simulations performed under varying particle total mass.

Figure 4.17 shows the amount of material entering the box. Here we could see the effect of the size of the box and the volume flow rate of the falling rocks. Initially, we opt for 300, 500 and 700 kg of material entering the box, but the collision between the rocks and the size of the box, make the latter to be filled only partially. This is to certify the reason why the force on the box represented in Figure 4.18 is not linear to the increase in mass, due to the diminution of the mass present.

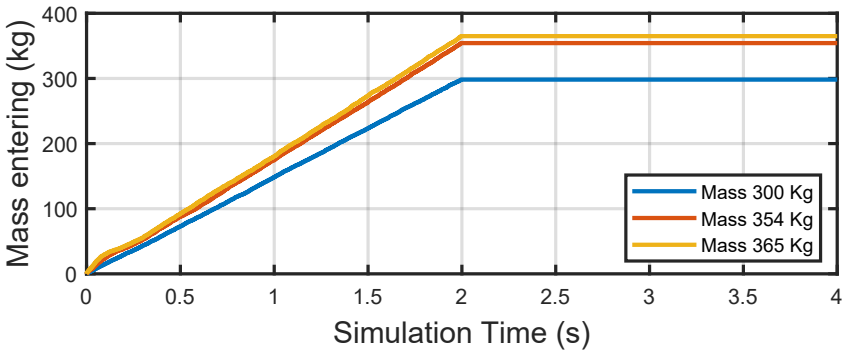


**Figure 4.17:** Total mass of rocks entering the box at a time-step $\Delta t_{DEM} = 5 \cdot 10^{-5}$s and a step-size $\Delta t_{MBD} = 10^{-3}$s.

In order to stay linear with the physical response obtained, in Figure 4.17 the real mass entering the system at each different case is represented. As could be seen from the Figure 4.17, the mass generation phase takes place during the first 2 seconds of the co-simulation. Also, in the legend attached there could be seen the real value of the mass entering the box.

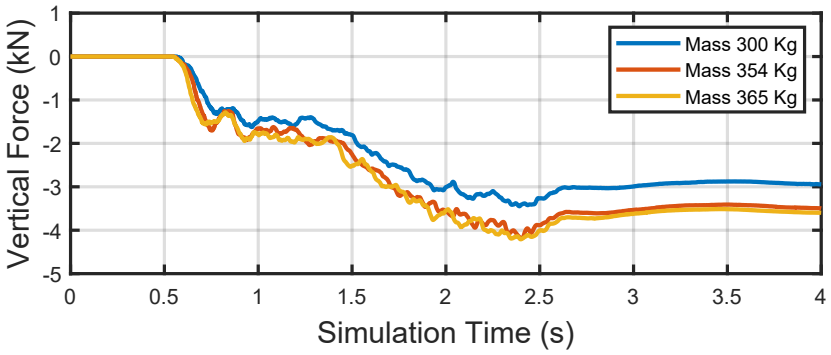


**Figure 4.18:** Force applied to the box in the vertical direction at a time-step $\Delta t_{DEM} = 5 \cdot 10^{-5}$s and a step-size $\Delta t_{MBD} = 10^{-3}$s for different masses entering the box.

Figure 4.18 represents the vertical force applied onto the box from the falling rocks. Note also, that the box is supported by a spring-damper system. As expected, the blue curve shows a lower vertical force than the other two curves due to the lower amount of mass introducing into the box.
In addition, as expected the kinetic and potential energy present in the system is higher for a bigger mass. The latter also affects the position of the box in the vertical direction, which is depicted in Figure 4.21.

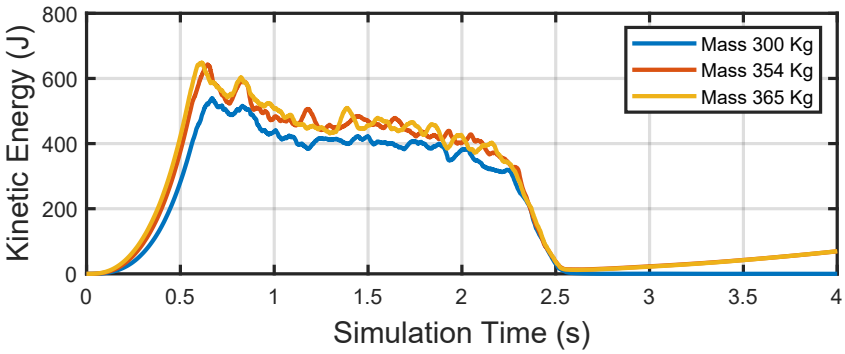


**Figure 4.19:** Total Kinetic Energy of the whole rock particles at a time-step $\Delta t_{DEM} = 5 \cdot 10^{-5}$s and a step-size $\Delta t_{MBD} = 10^{-3}$s for different masses entering the box.

The Kinetic Energy could be seen in Figure 4.19, where a similar trend for the different masses could be seen, and spikes could be seen when the rocks are falling into the box, making the trend complex, but still physically reliable. Also, note that for a Mass of 365 kg the system undergoes an overall interface instability.
Alongside the Kinetic Energy, Potential Energy is shown in Figure 4.20. We start at 0 level of potential energy then increasing with the rock height and the time they fall. Once, the stability is reached and a converging trend could be seen from second 2.5 and onward. Anyhow, the energy as could be seen is negative. This happens due to the movement of the box in the negative vertical direction, hence leading to a negative value of the Potential Energy.

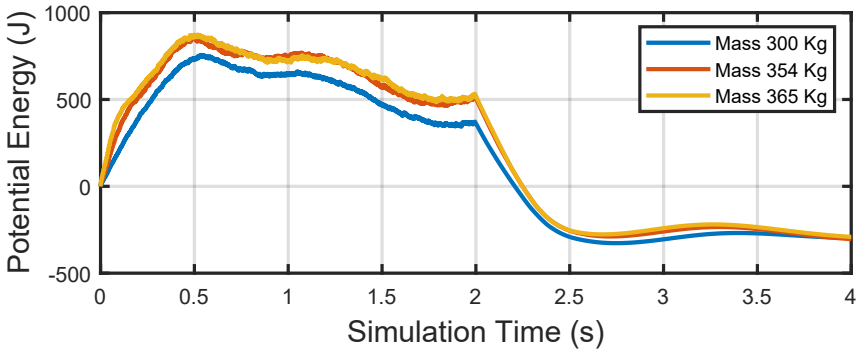


**Figure 4.20:** Total Potential Energy of the whole rock particles at a time-step $\Delta t_{DEM} = 5 \cdot 10^{-5}$s and a step-size $\Delta t_{MBD} = 10^{-3}$s for different masses entering the box.

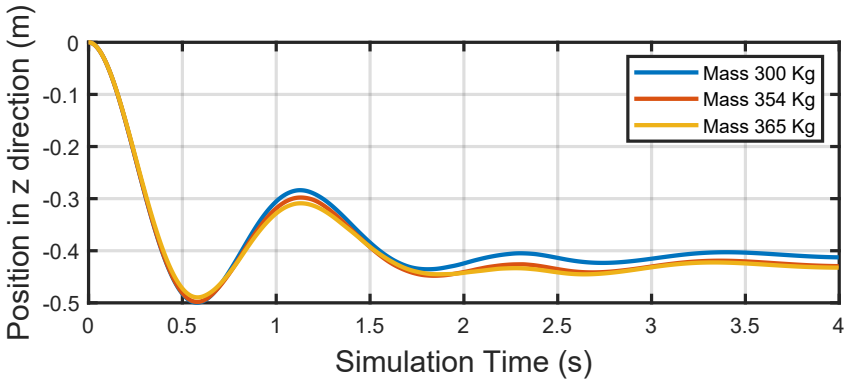


**Figure 4.21:** Position of the box in the vertical direction at a time-step $\Delta t_{DEM} = 5 \cdot 10^{-5}$s and a step-size $\Delta t_{MBD} = 10^{-3}$s for different masses entering the box.

Figure 4.21 instead represents the position of the box in the vertical direction, which as expected moves downwards due to the force exerted by the rocks mass. Note that the converging point of the box, is directly dependent on the spring constant coefficient. As we choose to keep a constant value for all the simulations performed the results that could be seen from the Figure 4.21, are only related to the mass entering the system, hence depending on the mass variation.

On the other hand, apropos of the box velocity, the mass entering the system has a negligible effect to the frequency or amplitude variation, leading to a rather negligible overall impact.

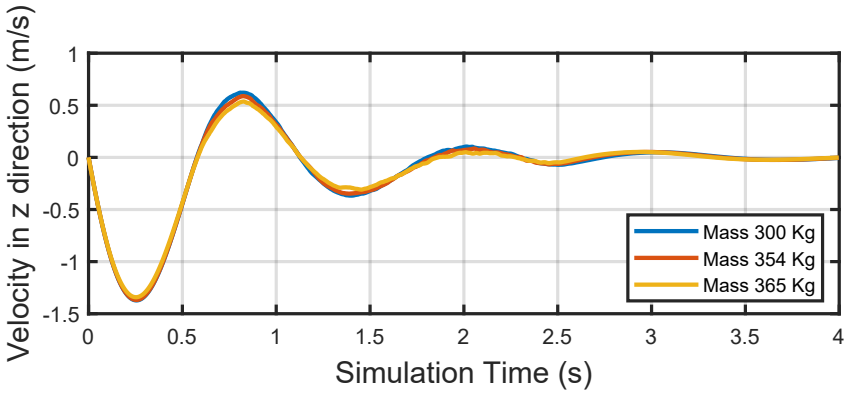


**Figure 4.22:** Velocity of the box in the vertical direction at a time-step $\Delta t_{DEM} = 5 \cdot 10^{-5}$s and a step-size $\Delta t_{MBD} = 10^{-3}$s for different masses entering the box.

### 4.2.3 Particle size examination

This section focuses in evaluating the particle size effects in the physical parameters we are looking into. The approach is the same as that of Section 4.2.2. Three different rocks mean radius are introduced, respectively $R_{m1} = 0.060$m, $R_{m2} = 0.090$m and $R_{m3} = 0.120$m. Instead, table 4.4 introduces all the non-varying parameters which are being used in the co-simulations which results are to be shown in the following pages.

| | |
|---|---|
| $\Delta t_{DEM}$ | $5 \cdot 10^{-5}$ s |
| $\Delta t_{MBD}$ | $10^{-3}$ s |
| Box density | 1000 kg/m$^3$ |
| Introduced mass | 250 Kg |
| Young's modulus | 100 MPa |
| Translational spring stiffness | 25000 $\frac{N}{m}$ |
| Damping coefficient | 2000 $\frac{N}{m/s}$ |

**Table 4.4:** Constant parameters for the simulations, which results can be seen in Figures 4.23, 4.24, 4.25, 4.26 and 4.27.

The figures represented below depict the effect of particle size in the convergence of the simulation technique used. In Figure 4.23 there is represented the force applied on the box in the vertical direction at different rock mean radius. The results show a very small dependence of the rock mean radius to the force obtained. But, this could be also due to the fact that the mean radius variation is small when compared to the bucket size and the mass introduced to the system, therefore the results are difficult to diverge at different values. Bigger sizes of rocks could lead to possible physical results fluctuations, but anyhow without affecting the validity and the fidelity of the interface.

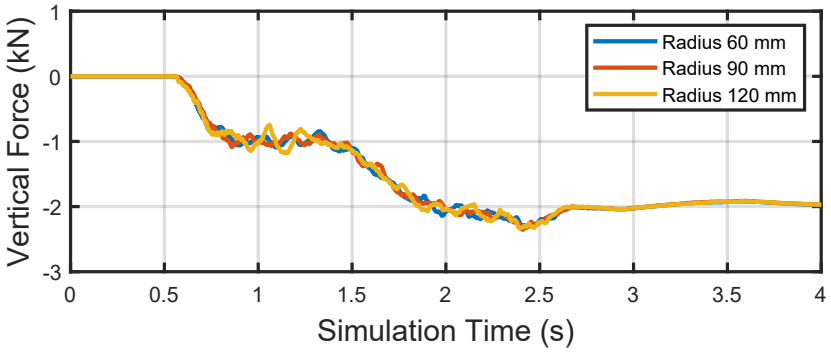


**Figure 4.23:** Force applied to the box in the vertical direction at a time-step $\Delta t_{DEM} = 5 \cdot 10^{-5}$s and a step-size $\Delta t_{MBD} = 10^{-3}$s for different rock particle sizes.

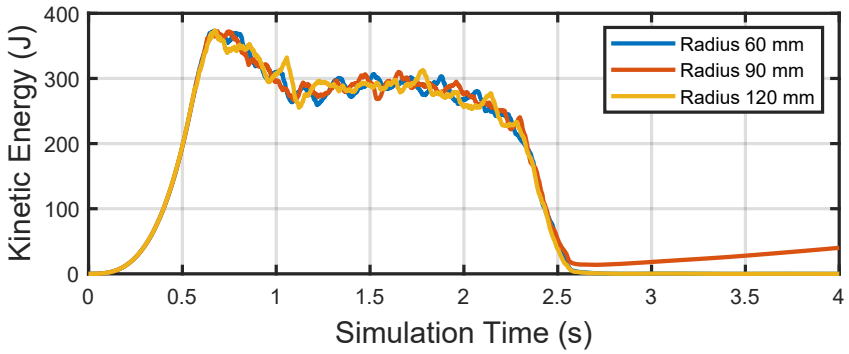


**Figure 4.24:** Total Kinetic Energy of the whole rock particles at a time-step $\Delta t_{DEM} = 5 \cdot 10^{-5}$s and a step-size $\Delta t_{MBD} = 10^{-3}$s for different rock particle sizes.

In addition to Force, there is possible to see the effect the rocks mean radius has on the Kinetic and Potential Energy, respectively shown in Figures 4.24 and 4.25. Kinetic Energy shows a very small dependency on the particle size chosen, thus the reason could be the same as the one regarding the force in the vertical direction. Anyhow, in Figure 4.24 a divergence of the Kinetic Energy could be seen in the end of the simulation when a rock mean radius of 90mm is chosen. This could be prone to the interface instability, which is also the main contributor to the fluctuating effect in Figure 4.24.
As regards the Potential Energy, it has a very converging trend for any of the chosen sizes. But, as expected it tends to diverge during the end of the simulation, as it did for the Kinetic Energy, when a rock mean radius of 90mm is being used. Other than that, the Potential Energy as expected, also in this case reaches a negative value, due to the negative displacement of the overall system, containing the rocks and the box, in the end of the simulation.

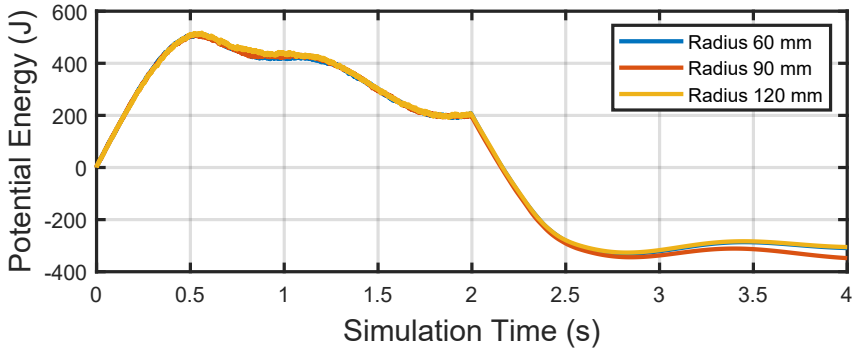


**Figure 4.25:** Total Potential Energy of the whole rock particles at a time-step $\Delta t_{DEM} = 5 \cdot 10^{-5}$s and a step-size $\Delta t_{MBD} = 10^{-3}$s for different rock particle sizes.

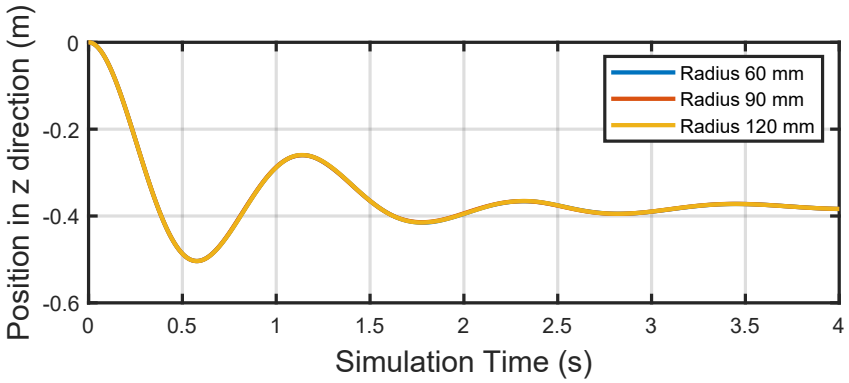


**Figure 4.26:** Position of the box in the vertical direction at a time-step $\Delta t_{DEM} = 5 \cdot 10^{-5}$s and a step-size $\Delta t_{MBD} = 10^{-3}$s for different rock particle sizes.

As we can see for each of the performed simulations the dependence on particle size is relatively small and negligible, as we reach a converging curve for the physical parameters of interest. The box velocity and position remain quite unaffected from the variation of the rock dimension. In Figure 4.26 the box starts at at a 0 vertical position then we could see a vertical negative displacement due to the weight of the box itself, which in turn is supported by the spring-damper system, and over time it tries to reach a converging and stable point trend when the rocks are entering it. A final convergence point could be seen when we reach 3 seconds of the simulation. The latter is furtherly confirmed when referring to the velocity in the vertical direction represented in Figure 4.27, which tries to settle down and reach a converging velocity of approximately 0 m/s after 4 seconds of simulation.

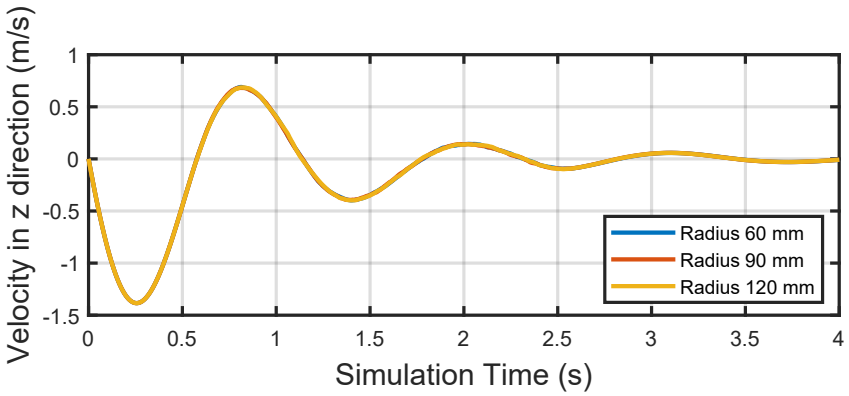


**Figure 4.27:** Velocity of the box in the vertical direction at a time-step $\Delta t_{DEM} = 5 \cdot 10^{-5}$s and a step-size $\Delta t_{MBD} = 10^{-3}$s for different rock particle sizes.

# 5

# Bucket load predictions

## 5.1 General load cases data and components

In this chapter the focus is representing the final results. The implementation of the overall interface reliability is discussed. The dynamics of the wheel loader in Simulink® and of the bucket to particles coupling is verified after each co-simulation set-up. Two versions of simulation cases are being introduced in each of the two sections, 5.2 and 5.3. But, let us first have a visual representation of the bucket itself. Subsequently, Figure 5.1 shows a sketch of the bucket in two different standpoints. Beyond, Figure 5.2 gives a 3D representation of the bucket, in IPS Demify®.

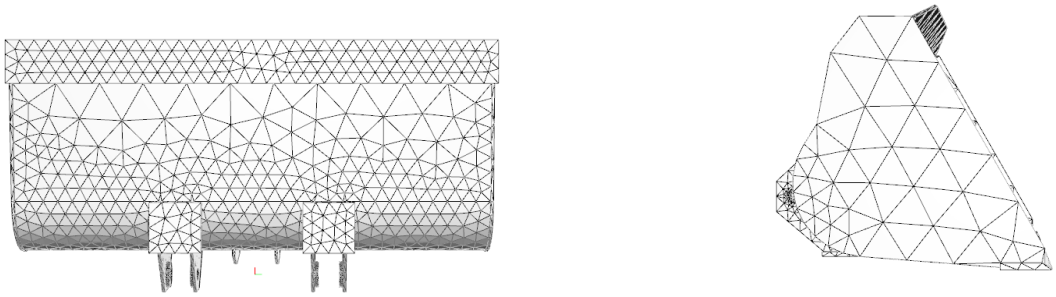

(a) Scene in x-y plane.

(b) Scene in x-z plane.

**Figure 5.1:** The sketch of the bucket used in the final simulations reported in Sections 5.2 and 5.3.

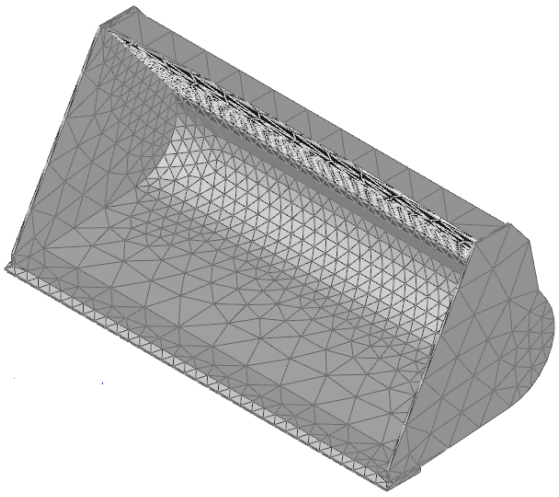

**Figure 5.2:** A 3-D representation of the bucket used in the simulations reported in Sections 5.2 and 5.3.

Both the Figures show the geometry mesh of the bucket. Bigger meshes could be noticed in planar surfaces, whereas much smaller mesh size at the corners and areas where the dynamical load prediction is more difficult. As regards the time steps, a DEM time-step $\Delta t_{DEM} = 5 \cdot 10^{-5}$s is used, whereas a MBD step-size $\Delta t_{MBD} = 10^{-3}$s is chosen.

## 5.2 Vertical loading of stand still machine

In order to have an understanding of the physics between the bucket and the rocks, the choice of having a simple bucket to rock interaction seems a reasonable approach, so the converging forces and moments are clearly seen and thus assuring the coupling method fully converges.

That being said, in this section a simulation in which a vertical falling of the rocks into the bucket for a specified interval of time is being carried out. This stand still bucket course precedes a vertical movement of the bucket and the particles inside it. Following the dynamics of the rocks and the bucket, we get a full record of the forces, moments and velocities present in the system.

As previously mentioned, the communication time step and step-size are respectively $\Delta t_{DEM} = 5 \cdot 10^{-5}$s and $\Delta t_{MBD} = 10^{-3}$s. In addition, a rock density of 1000 kg/m$^3$ is chosen, followed by a steel density of 7000 kg/m$^3$, both with a Poisson's ratio of 0.25. As regards, the rock to rock interaction a friction coefficient of 0.6 is chosen, followed by a restitution coefficient of 0.15. Instead, the rock to bucket interaction is composed of friction coefficient of 0.4, alongside a restitution coefficient of 0.15. The bucket is initially positioned at a rotated angle of 65° with respect to the y-axis. On the other hand, the rocks have a mean size diameter of 75 mm, with a lower and upper limit of 60 mm and 90 mm. Besides the particles are gener-

ated for a time duration of 1 second, frequency of 200 Hz and a mass rate of 180 kg/s.

Having introduced the set of specifications of the simulation, the obtained physical parameters are to be represented. The figures shown below give a visual feedback related to the kinematics of the system.

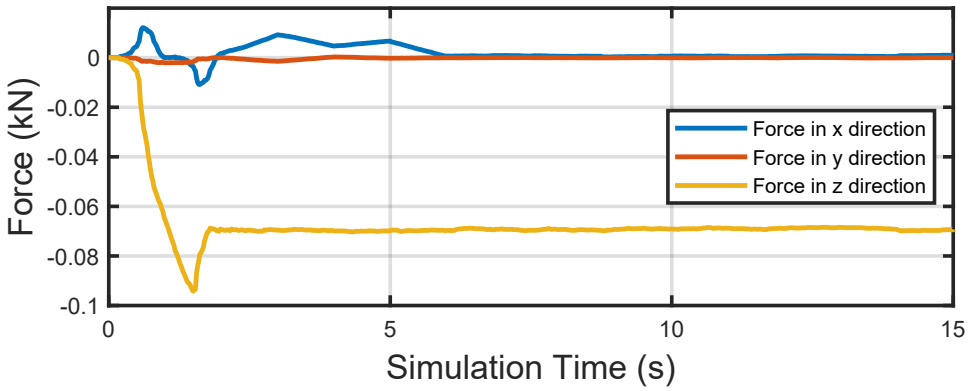


**Figure 5.3:** Force exerted on the bucket in all the directions while performing a vertical loading simulation.

Figure 5.3 represents the force applied on the bucket in all the directions. As expected, the amount of the force in the vertical direction is the major constituent. The impact of the rocks to the bucket is a main contributor to the graph, and it could be noted that in the first seconds of the simulations there is a bump of vertical force. This force reaches a stable and converging point as soon as the rocks stop falling and thus the vertical force applied to the bucket could be associated solely with the weight of the rocks. Also note the trend of the blue curve representing the Force in the longitudinal direction. That comes due to the contact between the rocks and the bucket itself, having the latter lifted, the overall impact of the falling rocks inside the bucket cause a slight movement of the bucket in the positive and negative direction, which comes from the presence of a force in that direction. Anyhow, this force reaches a zero trend as soon as the rocks are fully generated.

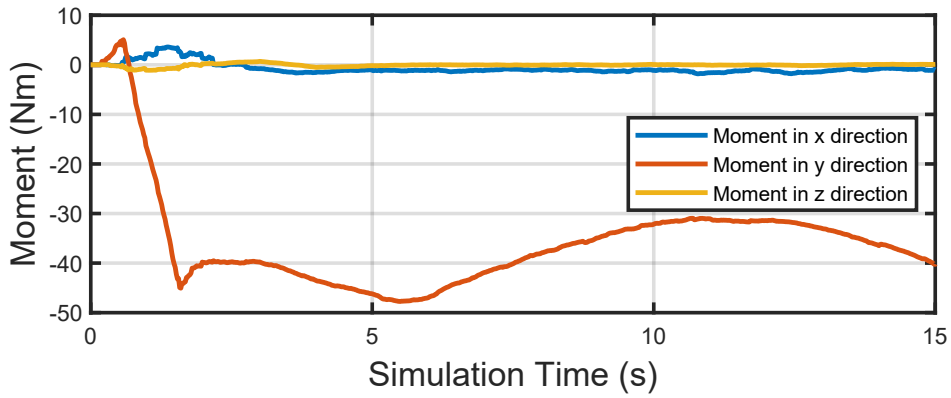


**Figure 5.4:** Moment applied on the bucket while performing a vertical loading simulation.

Figure 5.4 instead, represents the moment progress over simulation time. It can be clearly seen its dependence to the forces being applied to the bucket. Also, in this graph we see the partition of the moment in all the 3 directions, with a major reach in the y direction. Note that during the last 10 seconds of the co-simulation a moment change could be observed. This comes due to the lifting of the bucket in the vertical direction, hence leading to a movement of the rocks inside the bucket, which in turn give rise to a variation applied in the y direction. Another thing of interest, is the slight moment there is present around the x direction mainly in the initial stage of the simulation, which is prone do the minimal mass variation present inside the bucket with respect to its center line standing in the middle of the bucket.

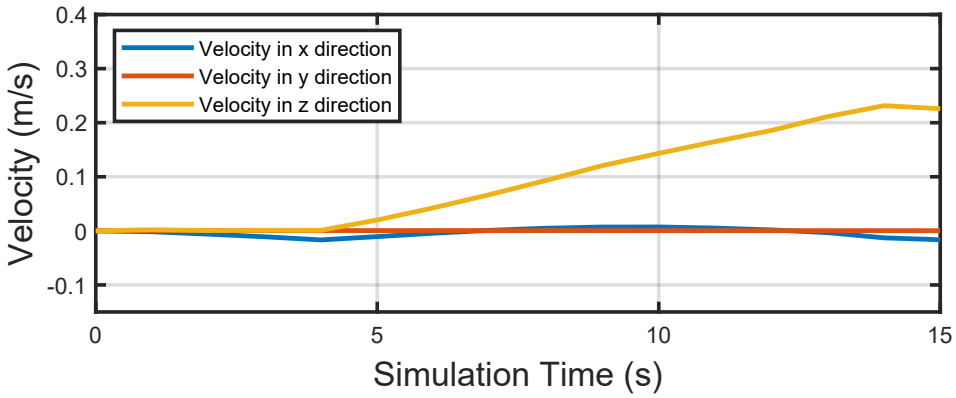


**Figure 5.5:** Velocity of the bucket in all directions while performing a vertical loading simulation.

On the other hand, the velocity of the bucket is represented in Figure 5.5. Velocity is the parameter which is computed in Simulink® and right after transmitted to Demify®, which promptly updates the force applied to the bucket, via the DEM solver. It could be observed that in x direction the presence of an impact force due to the rocks slightly varies the wheel loader velocity. Anyhow, the main velocity rise comes with the hydraulics which lifts the bucket.

## 5.3 Horizontal loading of the machine

In this second example, the simulation conditions are marginally modified. The mean size of a rock particle is $R_{mean} = 0.4$m, accompanied by a Poisson's ratio of 0.28, Young's modulus of 10 MPa and density of $2700\frac{kg}{m^3}$. The total amount of rock material is 6500 Kg. As regards the time step and step-size, they remain the same, the DEM time-step is $\Delta t_{DEM} = 5 \cdot 10^{-5}$s and the MBD step-size is $\Delta t_{MBD} = 10^{-3}$s. In this instance, the wheel loader performs a horizontal movement into a pile of rocks, as might be seen in Figure 5.6. Here, the particle to particle and particle to bucket interaction is more integral so a more elaborate inspection of the forces, moments and velocities could be conducted.
Figures 5.7, 5.8 and 5.9 show the co-simulation results from Simulink, whereas Figure 5.6 shows an instant of the co-simulation in IPS Demify.

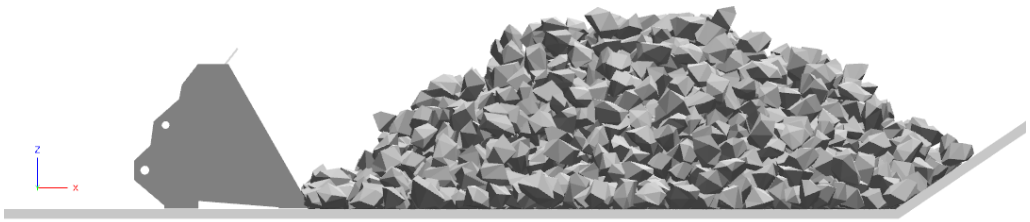

**Figure 5.6:** A visualization in x-z plane of the bucket entering a pile of rocks, loading and exiting from it in the negative x-direction.

The simulation time is set to be 20 s, which is the time the bucket enters the pile, withdraws the material and then leaves the pile.

Figure 5.7 shows the forces applied on the bucket in all the directions. As expected, there is almost no force present in the y-direction. The interaction between the bucket and rocks occurs mainly in the longitudinal-x and vertical-z directions. Note that, there is a high presence of force in the longitudinal direction, due to the presence of a huge amount of rocks, which weight makes it difficult for the bucket to move forward. This force tends to converge to zero, when the bucket performs a vertical loading movement. At this point, there is a presence of force in the vertical direction, which then converges to the force applied by the weight of the material

remaining inside the bucket until the end of the simulation. In the trend of the vertical force, two spikes could be noticed. This comes to the material movement inside the bucket, when a velocity gradient is applied onto the bucket. In other terms, some of the material inside the bucket lifts up when perceiving a quick change of the velocity of the bucket and then gets back into the bucket, leading to the same peak height, hence the same weight of material. The curve then performs a decreasing trend which comes due to the dropping of some of the rocks inside the bucket.

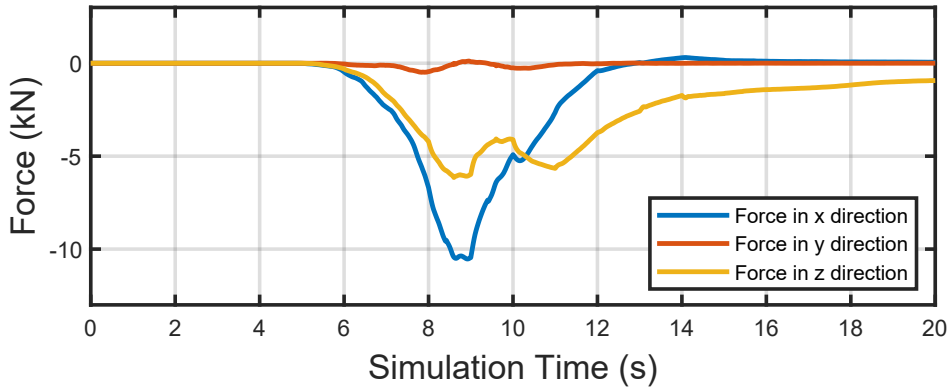


**Figure 5.7:** Force exerted on the bucket in all the directions while performing a horizontal loading simulation.

In Figure 5.8 instead, the moment in all directions is represented. A large moment value is present around y axis, since a high amount of load is applied in the x and z directions, making the rotation around y-axis difficult and heavy loaded, thus creating a moment around y-axis. Also in this case a moment spike could be noticed during the same simulation time, as present in the Force graph. As explained in advance, this is a result of the absent force, in this case in the vertical direction, which leads to a double spike formation. Anyhow, it is conserved, even though the moment around y-axis converges to a lower value due to the diminishing of the forces present, hence dropping of the rocks from the bucket.

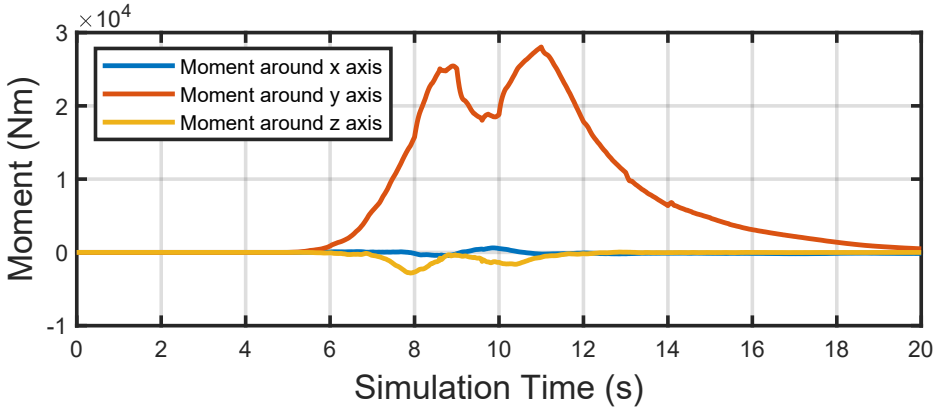


**Figure 5.8:** Moment applied on the bucket while performing a horizontal loading simulation.

On the other hand, Figure 5.9 depicts the velocity of the bucket in all the directions. To note, the velocity in the vertical-z direction when the bucket performs a lifting operation so to make the loading possible. The blue curve instead represent the overall bucket movement in the longitudinal direction, where a positive trend could be seen when approaching the pile to make the loading possible, and a negative trend could be seen after the loading is performed. Instead, there is no velocity present in the y direction.

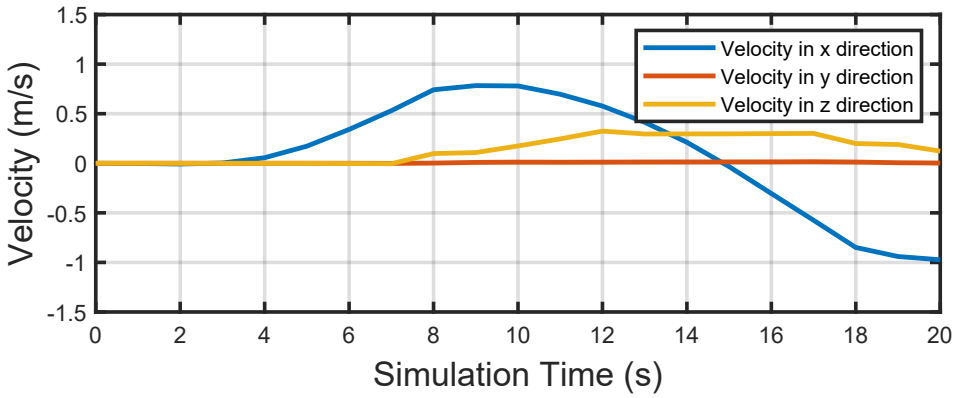


**Figure 5.9:** Velocity of the bucket in all directions while performing a horizontal loading simulation.

Overall, the results obtained from the loading operation cases represent a verification step when it comes to the functioning of the coupling between Demify® and Simulink®.

# 6
# Conclusion

## 6.1 Discussion

The procedure deployed in this research adjusts to the different simulation cases, depending on the needs related to the aim of a chosen project. In Chapter 5, simple material handling operations are performed. Although, the simulations could be additionally enhanced by implementing more elaborate wheel loader operations, the goal in this project is that of retrieving results, in terms of physical reliability and computational performance, hence a functioning coupling.

The co-simulation target is reached by developing a coupling technique derived by the use of Functional Mock-up Units, which stands as a solid bridge between the DEM solver Demify® and the MBD solver in Matlab/Simulink®. The pioneering step is the enactment of FMU, being the main ingredient of the whole recipe. The use of a new GPU solver for complex shaped particles, in this case non-convex polyhedrons, gives rise to high well-founded rock shape representation. *This*, in parallel with a firm DEM solver, making up for the interactions and motions between the rocks and the bucket, bring about a strong starting point for the solution. The latter is packed into FMUs being a suitable language for Simulink® where it is imported, making rise to a coupling between the two, where the communication per simulation is imminent.

Obtaining reliable results is not the only curb to take into consideration, because the computation performance is also of high interest. That being said, all the simulation strategy follows a DEM time step and MBD step-size analysis, where the simulation time is used as a performance checker throughout all the performed load cases, up to Chapter 5, where fixed values of DEM time step and MBD step-size are set.

## 6.2 Final Remarks

The challenges behind the design and co-simulation of heavy equipment machines start with the complex nature of the material these machines will face, followed by the remarkably high amount of particles generated per simulation. Keeping in mind the goal, which is to meet the needs of engineers, makes the process even more challenging and tempting. In addition to that, almost every aspect of a wheel loader's component performance is dependent to some degree to the material being handled. Hence, it is crucial to ensure a functional design to then opt for high performance

efficiency.

As a result, the study of the rock particle characterization is vital in this project as they stand behind the dynamics of the system. In addition, a work-flow for Demify® and Simulink® is developed. The strategy used in this work does not only verify a new approach to a reliable and computationally effective match of the reality via a virtual elaboration technology, but also puts into play new co-simulation performers such are FMUs, which stand as the new and reliable play makers of the software coupling methods.

# Bibliography


[1] *A GPU Polyhedral Discrete Element Method*; Bilock, Adam, 2020

[2] *A coupled multibody and discrete element approach for roller compaction dynamics*; Göransson Axås, Joar, 2020

[3] *Blaze-DEMGPU: Modular high performance DEM framework for the GPU architecture*; Govender, Nicolin and Wilke, Daniel N and Kok, Schalk; *SoftwareX*, volume 5, *Elsevier*, 2016

[4] *Collision detection of convex polyhedra on the NVIDIA GPU architecture for the discrete element method*; Govender, Nicolin and Wilke, Daniel N and Kok, Schalk; *Applied Mathematics and Computation*, volume 267, *Elsevier*, 2015

[5] *DEM modelling of industrial granular flows: 3D case studies and the effect of particle shape on hopper discharge*; Cleary, Paul W and Sawley, Mark L; *Applied Mathematical Modelling*, volume 26, *Elsevier*, 2002

[6] *Generation of an optimised master algorithm for FMI co-simulation*; Van Acker, Bert and Denil, Joachim and Vangheluwe, Hans and De Meulenaere, Paul; *SpringSim (TMS-DEVS)*, 2015

[7] *Hopper flow of irregularly shaped particles (non-convex polyhedra): GPU-based DEM simulation and experimental validation*; Govender, Nicolin and Wilke, Daniel N and Wu, Chuan-Yu and Khinast, Johannes and Pizette, Patrick and Xu, Wenjie; *Chemical Engineering Science*, volume 188, *Elsevier*, 2018

[8] *Modeling, validation and energy flow analysis of a wheel loader*; Kim, Hakgu and Oh, Kwangseok and Ko, Kyungeun and Kim, Panyoung and Yi, Kyongsu; *Journal of Mechanical Science and Technology*, volume 30, *Springer*, 2016

[9] *Co-simulation as a Fundamental Technology for Twin Ships*; Hatledal, Lars Ivar and Skulstad, Robert and Li, Guoyuan and Styve, Arne and Zhang, Houxiang; 2020

[10] *Modeling the particle breakage of rockfill materials with the cohesive crack model*; Ma, Gang and Zhou, Wei and Chang, Xiao-Lin ; *Computers and Geotechnics*, volume 61, *Elsevier*, 2004

[11] *Contact forces of polyhedral particles in discrete element method*; Nassauer, Benjamin and Kuna, Meinhard; *Granular Matter*, volume 15, *Springer*, 2013

[12] *Pyfmi: A python package for simulation of coupled dynamic models with the functional mock-up interface*; Andersson, Christian and Åkesson, Johan and Führer, Claus; *Centre for Mathematical Sciences, Lund University Lund*, 2016

[13] *Python for Computational Science and Engineering*; Fangohr, Hans; *Faculty of Engineering and the Environment University of Southampton*, 2015

[14] *Granular dynamics, contact mechanics and particle system simulations*; Thornton, Colin; *A DEM study. Particle Technology Series*, volume 24, *Springer*, 2015

[15] *Generation of functional mock-up units for co-simulation from simulink®, using explicit computational semantics: work in progress paper*; Pussig, Bart and Denil, Joachim and De Meulenaere, Paul and Vangheluwe, Hans; *Proceedings of the Symposium on Theory of Modeling and Simulation-DEVS Integrative*, 2014

[16] *Bucket-soil interaction for wheel loaders: An application of the Discrete Element Method*; Henriksson, Felix and Minta, Joanna, 2016

[17] *Simulation of soil-to-tool interaction using Discrete Element Method (DEM) and Multibody Dynamics (MBD) coupling*; Ghorbani, Sadaf; 2019

[18] *Co-simulation framework of discrete element method and multibody dynamics models*; Lommen, Stef and Lodewijks, Gabriel and Schott, Dingena L; *Engineering Computations*, *Emerald Publishing Limited*, 2018

[19] *A discrete element model and its experimental validation for the prediction of draft forces in cohesive soil*; Obermayr, Martin and Vrettos, Christos and Eberhard, Peter and Däuwel, Thomas; Journal of Terramechanics; volume 53, *Elsevier*, 2014

[20] *Coupling a DEM material model to multibody construction equipment*; Burger, M and Dressler, K and Ekevid, T and Steidel, S and Weber; *Proceedings of the ECCOMAS Thematic Conference on Multibody Dynamics*; 2017

[21] *Coupling DEM Particles to MBS Wheel Loader via Co-Simulation*; Matthias, Balzer and Burger, Michael and Dauwel, Thomas and Ekevid, Torbjörn and Steidel, Stefan and Weber, Dietmar; *4th International Commercial Vehicle Technology Symposium*; *Shaker Verlag*, 2016

[22] *Segregation of rock materials during unloading*; Quist, Johannes, Hunger, F., and Jareteg, K.; Fraunhofer-Chalmers Centre for Industrial Mathematics, Computational Engineering and Design. Göteborg, SBUF project 13638, 2019

[23] *Investigation of segregation effects and compaction of unbound rock materials*; Quist, Johannes, Jareteg, Klas, Bilock, Adam, and Persson, A; Fraunhofer-Chalmers Centre for Industrial Mathematics, Computational, Engineering and Design. Göteborg, SBUF project 13820, 2021

[24] *Shape representation of axi-symmetrical, non-spherical particles in discrete element simulation using multi-element model particles*; Favier, JF and Abbaspour-Fard, MH and Kremmer, M and Raji, AO; *Engineering Computations*, MCB UP Ltd, 1999

[25] *Shape representation and contact detection for discrete element simulations of arbitrary geometries*; Hogue, Caroline; *Engineering Computations*, MCB UP Ltd, 1998

[26] *Complete set of stochastic Verlet-type thermostats for correct Langevin simulations*; Gr∅nbech – Jensen, Niels; *Molecular Physics*, Taylor & Francis, 2020